Copy No. 243

RM No. L8A12

RESEARCH MEMORANDUM

FORCE, STATIC LONGITUDINAL STABILITY, AND CONTROL CHARACTERISTICS OF A $\frac{1}{16}$-SCALE MODEL OF THE BELL XS-1 TRANSONIC RESEARCH AIRPLANE AT HIGH MACH NUMBERS

By

Axel T. Mattson and Donald L. Loving

Langley Aeronautical Laboratory
Langley Field, Va.

NATIONAL ADVISORY COMMITTEE FOR AERONAUTICS

WASHINGTON

June 23, 1948

NATIONAL ADVISORY COMMITTEE FOR AERONAUTICS

RESEARCH MEMORANDUM

FORCE, STATIC LONGITUDINAL STABILITY, AND CONTROL CHARACTERISTICS OF A $\frac{1}{16}$-SCALE MODEL OF THE BELL XS-1 TRANSONIC RESEARCH AIRPLANE AT HIGH MACH NUMBERS

By Axel T. Mattson and Donald L. Loving

SUMMARY

This report contains complete results obtained to determine the effects of compressibility at high Mach numbers on a $\frac{1}{16}$-scale model of the Bell XS-1 transonic research airplane and therefore supersedes NACA RM No. L7A03 which was previously prepared at the Langley 8-foot high-speed tunnel.

These results are presented for several model configurations through a Mach number range from 0.4 to approximately 0.95. All the data have been corrected for tare forces.

At a Mach number of 0.78 a drag force break occurs for the high-speed level-flight lift coefficient ($C_L = 0.1$). This force break is accompanied by a rapid increase in drag coefficient with increase in speed. At a Mach number of 0.925 the drag coefficient is about five and one-half times the subcritical value. A lift force break occurs at a Mach number of 0.80 for an angle of attack of 0°. At a Mach number of 0.875 the lift coefficient decreases rapidly to approximately zero. At a Mach number of 0.925, the lift coefficient increases again to a value of 0.2.

This configuration has a high degree of constant-speed static longitudinal stability except for a narrow range of Mach numbers (approximately 0.875 to 0.90) at low lift coefficients.

Stabilizer and elevator effectiveness tend to decrease at the high Mach numbers, but no serious control problems are expected up to the highest Mach number investigated because the lowest degree of effectiveness is still of such magnitude as to be able to produce changes in trim for level flight at the desired altitudes.

Tuft surveys of the aft portion of the fuselage showed no separation or unusual flow patterns up to a Mach number of 0.925 for a maximum angle of attack of 3° and a maximum yaw angle of 2.2°.

The results show that the speed-retarding brakes are barely capable of reducing the terminal velocity of the airplane to the critical Mach number range.

INTRODUCTION

This report supersedes the results presented in reference 1 and pertains to data relative to the force and longitudinal stability and control characteristics of a $\frac{1}{16}$-scale model of the Bell XS-1 transonic research airplane at high Mach numbers. The tests were conducted in the Langley 8-foot high-speed tunnel at the request of the Air Materiel Command, Army Air Forces.

At the time of the XS-1 model investigation, for which results were published in reference 1, difficulty was experienced in obtaining tare data. It was no less difficult to obtain tare corrections for the present results, but prior to the tests a more sensitive balance system was installed and during the test program sufficient tare configurations were included to correct all configurations of the regular model investigated. The more sensitive balance system was used for the regular model testing also. Therefore, this report will supersede the results qualitatively presented in reference 1.

The results presented herein were obtained for the model without the simulation of rocket power. Angles of attack of -2°, 0°, 3°, and 6° were investigated, as well as stabilizer settings of -3°, 0°, and 3° and elevator deflections of -3°, 0°, 3°, and 6°. The aerodynamic characteristics of a fuselage speed-reduction brake were also investigated. Visual observations were made of woolen tufts located on the fuselage side aft of the wing trailing edge as an indication of any flow disturbance in this region.

SYMBOLS

The symbols used in this report and their definitions are as follows:

V	free-stream velocity, feet per second
ρ	free-stream density, slugs per cubic foot
q	dynamic pressure, pounds per square foot $\left(\frac{1}{2}\rho V^2\right)$
a	velocity of sound, feet per second ($49.0\sqrt{T}$, T in $^\circ$F absolute)

M Mach number $\left(\frac{V}{a}\right)$

L lift, pounds

D drag, pounds

M_{cg} pitching moment, about center of gravity (25 percent $\bar{c}$), foot-pounds

S_w wing area, 0.508 square foot

$\bar{c}$ mean aerodynamic chord, 3.607 inches

$C_L = \frac{L}{qS_w}$

$C_D = \frac{D}{qS_w}$

$C_{m_{cg}} = \frac{M_{cg}}{qS_w\bar{c}}$

α angle of attack measured with respect to fuselage center line, degrees

i_t angle of incidence of the horizontal tail with respect to fuselage center line, degrees

δ_e elevator angle with respect to horizontal-tail chord line, degrees

ϵ effective downwash angle, degrees

X' distance from center of gravity to aerodynamic center of wing-fuselage combination (positive when center of gravity is rearward)

ψ yaw angle measured with respect to fuselage center line (positive with right wing retarded), degrees

$\left(\frac{dC_m}{dC_L}\right)_w$ static longitudinal stability of the wing-fuselage combination

$\frac{\partial C_L}{\partial \alpha}$ lift-curve slope of the wing-fuselage combination

$\frac{d\epsilon}{dC_L}$ rate of change of downwash at the tail with lift of the wing

$\left(\frac{\partial C_L}{\partial \alpha}\right)_t$ lift-curve slope of the horizontal tail

Subscripts:

t horizontal tail

w wing–fuselage combination

AIRPLANE, APPARATUS AND METHODS

Airplane and Model

The Bell XS–1 is a single–place, straight midwing research airplane designed for extreme variations in speed, wing loading, and altitude. The airplane employs a rocket motor and is equipped with an adjustable power–driven stabilizer.

A $\frac{1}{16}$-scale, all–metal, solid–construction model, which consisted of a wing, fuselage, and empennage, was supplied by the Bell Aircraft Corporation for this investigation. The principal dimensions of the Bell XS–1 research airplane as tested in the Langley 8–foot high–speed tunnel are shown in the three–view drawing in figure 1. The physical characteristics of the airplane are given in table I. The speed–reduction brakes supplied by the NACA were made of solid duralumin and located on the side center line of the fuselage aft of the wing trailing edge as shown in figure 1. The model stabilizer could be set for incidence angles of $\pm 6^\circ$, $\pm 3^\circ$, and 0°. Horizontal tails with built–in elevator settings, leaving no gaps between the stabilizer and elevator, were supplied for the elevator deflections.

Apparatus and Methods

The Langley 8–foot high–speed tunnel, in which this investigation was conducted, is a single–return, closed–throat type capable of obtaining – tunnel empty – a Mach number of unity in the test section. The tunnel air velocity is continuously controllable. For this investigation, Mach numbers up to approximately 0.95 were obtained by the use of a sting–support system.

Tunnel sting–support system.– In order to dispense with the interference effects of conventional support struts at high Mach numbers and to permit model testing at a Mach number approaching unity, the model was mounted on a sting–support system as shown in figure 2. The sting support extended from the rear of the fuselage to a shielded strut mounted vertically and connected to the tunnel balance system. The sting shield extended 2.60 inches in front of the vertical support–strut fairing. A smooth fairing was located on the sting directly in

front of the gap between the sting and sting shield in order to prevent direct flow into the support shield. Figure 2 shows the sting-support system and also the tare setup in the Langley 8-foot high-speed tunnel test section.

Tare setup and evaluation.- Auxiliary arms to support the model as shown in figure 2 were used to determine the tare values of the support system and interference effects. The supports in the region of the model were 6-percent-thick airfoils swept back 30° to minimize interference effects and delay effects due to compressibility for the test Mach number range. The remaining parts of the tare supports were thin plates extending back and connected to the support strut.

The tare setups and the method by which all the data presented in this report have been corrected are illustrated in figure 3. Guy wires from the wing tips were used on all tare runs so that the system would be rigid when no sting was used. Three model tare configurations were required to evaluate the tare forces. For the tare configuration without the sting, the sting was replaced by a small fuselage fairing. This fairing was relatively blunt because of the geometry of the fuselage contours, and also, it was believed that a longer fuselage fairing would change the basic pitching-moment characteristics of the fuselage. The assumptions included in the tare evaluation are that the interference effects of arms on sting and sting on arms are negligible.

In order to indicate the magnitude of the effects of the tares on the pitching-moment coefficient of the XS-1 model, figure 4 has been prepared for angles of attack of 0° and 3°.

TESTS AND MEASUREMENTS

Test Conditions

These tests were run through a Mach number range from 0.4 to approximately 0.95. The model Reynolds number ranged for these tests from approximately 1.03×10^6 to 1.8×10^6 and was based on a model mean aerodynamic chord of 3.607 inches.

Measurements

The force measurements are presented as standard NACA nondimensional coefficients. These coefficients are based on a model wing area of 0.508 square foot. The pitching moments were taken about a center-of-gravity position (0.25$\bar{c}$) indicated in figure 1, which also gives

the principal dimensions of the model as tested in the Langley 8-foot high-speed tunnel. The following model configurations were tested:

(a) Model less wing with and without horizontal tail

(b) Model less horizontal tail

(c) Complete model with

$$i_t = 0^\circ, \delta_e = -3^\circ$$

$$i_t = 0^\circ, \delta_e = 0^\circ$$

$$i_t = 0^\circ, \delta_e = 3^\circ$$

(d) Complete model with

$$i_t = -3^\circ, \delta_e = 0^\circ$$

$$i_t = 3^\circ, \delta_e = 0^\circ$$

$$i_t = 3^\circ, \delta_e = -3^\circ$$

(e) Complete model with

$$i_t = 3^\circ, \delta_e = 3^\circ$$

$$i_t = 3^\circ, \delta_e = 6^\circ$$

(f) Model less horizontal tail with speed-reduction brake

(g) Complete model with speed-reduction brake

CORRECTIONS

Because of the relatively small model required for testing at high Mach numbers, wind-tunnel corrections such as model constriction and wake constriction are small up to the highest test Mach number attained. An estimation of the tunnel correction, obtained by using methods described in references 2, 3, 4, and 5, indicates that the corrections to the Mach number will be approximately 1.5 percent at a tunnel Mach number of 0.9 for the highest lift coefficients attained. Corrections in dynamic pressure will be of the same order of magnitude. The lift vortex-interference correction is small, being a change in angle of attack of less than 0.1° at the highest lift coefficient obtained. Because of the small magnitude of the corrections, they have not been applied to the data presented herein.

Tunnel-wall pressure measurements showed that the flow in the test section was free of interference from tunnel choking effects and from the flow field of the support strut at the highest Mach number for which data are presented.

The model was accurately constructed and, being of all-metal construction, remained the same throughout the investigation. Displacement of the model center of gravity relative to the trunnion axis of the tunnel due to air loads was continuously observed by the use of a cathetometer. Corrections for model displacements have been applied to the pitching moments. The angle of attack of the model was also checked by the use of the cathetometer; for the maximum loads obtained the change in angle of attack due to deflection of the model was of the order of 0.2°. The deflections were considered negligible for the angle-of-attack range investigated.

RESULTS AND DISCUSSION

Aerodynamic Characteristics

Drag characteristics.- Figure 5 presents the variation of angle of attack and drag coefficient with lift coefficient for the complete model through a Mach number range from 0.4 to 0.925. The variation of drag coefficient with Mach number for lift coefficients of 0.1 and 0.4 is shown in figure 6. Figure 6 also indicates a complete model drag-coefficient value of 0.0155 for a lift coefficient of 0.1 at a Mach number of 0.6. When the Mach number increases to approximately 0.78, a drag force break occurs for the high-speed level-flight lift coefficient ($C_L = 0.1$). This force break is followed by a rapid increase in drag coefficient with increase in Mach number. At a Mach number of 0.925 the drag coefficient reaches a value of approximately 0.083 which is about five and one-half times the subcritical value. Figure 6 also indicates a lift force break at a Mach number of 0.765 for a lift coefficient of 0.4. The rapid drag-coefficient rise that follows results in a value of approximately 0.1055 at a Mach number of 0.925.

Lift characteristics.- The variation of lift coefficient with Mach number for angles of attack of -2°, 0°, 3°, and 6° is presented in figures 7 and 8 for all model configurations investigated. At an angle of attack of 0° the lift force break for the complete model occurs at a Mach number of 0.80. For this condition the model lift coefficient is approximately 0.30. With increase in Mach number to 0.875 the lift coefficient decreases rapidly to approximately zero. With a further increase in Mach number to 0.925, the lift coefficient increases again to 0.2. This increase in lift coefficient at high supercritical Mach numbers, although subject to more fundamental investigation, is believed to be mainly the result of the rearward movement of the shock disturbance on the upper surface of the wing.

Pitching-moment characteristics.- Figures 7 and 8 also present the pitching-moment coefficients for constant angles of attack against Mach number. For all the configurations presented, no large changes in the pitching-moment variation with Mach number occur until a Mach number of 0.85 is reached. Thereafter, from a Mach number of 0.85 to approximately 0.95, large changes in pitching moment occur. These changes in pitching moment occur with relatively small increases in Mach number.

Aerodynamic characteristics of a speed-reduction brake.- Figure 9 presents the variation of incremental drag, lift, and pitching-moment coefficients with Mach number due to the addition of a speed-reduction brake on the XS-1 with and without horizontal tail. The variation for all practical purposes is essentially the same throughout the Mach number range tested; that is, up to a Mach number of 0.925, the limit for these tests. The model configuration was tested at an angle of attack of -2° which represents approximately the zero-lift condition.

If a wing loading of 40 pounds per square foot is assumed, the terminal Mach number of the XS-1 with speed-reduction brakes extended 65° is found to be approximately 0.83 or around 598 miles per hour at 15,000 feet. Without the speed-reduction brakes, the terminal velocity would correspond to a Mach number of 0.93 or 670 miles per hour. This shows a 10.75-percent reduction in terminal velocity due to the brakes and indicates that the brakes are barely capable of reducing the speed of the model to the critical Mach number range.

Figure 9 shows that the lift increment produced by the speed-reduction brakes is negligible.

The incremental pitching-moment coefficient due to the speed-reduction brakes, figure 9, shows that at a Mach number of approximately 0.85 a diving moment is produced and with a further increase in Mach number this diving moment has decreased so that at a Mach number of 0.94 a pull-out moment is indicated. The same trend is shown for the model without horizontal tail except that the pull-out moment at a Mach number of 0.94 is somewhat less than that with the horizontal tail.

Tuft survey.- Woolen tufts were placed on the side of the fuselage in the area between the wing trailing edge and the extreme tail end of the model. Neither separation nor unusual flow patterns were noted for the configurations tested throughout the Mach number range. The configurations observed were as follows:

α	i_t	δ_e	ψ
0.1°	0°	0°	0°
3°	0°	6°	0°
3°	0°	6°	2.2°

Static Longitudinal Stability Characteristics

The static longitudinal stability characteristics for the complete model with $i_t = 0^\circ$, $\delta_e = 0^\circ$ are presented as the variation of pitching-moment coefficient with lift coefficient for Mach numbers from 0.40 to 0.925 in figure 10. The usually expected stability increase with Mach number increase is indicated for the positive lift-coefficient range. The slope of the pitching-moment curve $\left(\partial C_m/\partial C_L\right)_M$ is approximately −0.08 at a Mach number of 0.40 and increases to about −0.16 at a Mach number of 0.925. In the negative lift-coefficient range investigated, however, the trend is quite different. For the stabilizer setting (of 0°) the model becomes unstable in this negative C_L range between approximate Mach numbers of 0.85 to 0.90. In figures 11 to 13 this same trend may be noted for all stabilizer and elevator settings tested. It should be noted that the analysis made herein is for an untrimmed condition and the airplane may or may not experience difficulty depending on the flight plan. However, it should be noted (in fig. 11) that for a Mach number of 0.875, a lift coefficient of about 0.04, and a stabilizer angle for trim of approximately 3.0, the airplane is statically unstable. Because of the limited range of lift coefficient and Mach number, the seriousness of this instability may be questionable. However, because of the very low lift coefficients attained in sea level flight (fig. 20), it would probably make flight in the Mach number range very near to the ground hazardous because of the danger of overcontrolling. Heretofore the general longitudinal stability characteristics in the supercritical speed range indicated an increasing stability with Mach number at low lift coefficients, as well as high lift coefficients, up to the stall. The present investigation indicates that an unstable region in the low or negative lift-coefficient range at higher supercritical Mach numbers does exist for this configuration.

Contribution of various components to constant-speed longitudinal stability.- The following analysis has been made to determine qualitatively the magnitude of the contribution of the various components in the approximate static longitudinal stability equation to the unstable condition indicated for the XS-1 airplane in the range of low lift and high speed. In order to ascertain the component contributing most, each principal component of the general stability equation for the complete airplane has been obtained and evaluated. The approximate constant-speed static longitudinal stability equation used is as follows:

$$\frac{dC_m}{dC_L} = \left(\frac{\partial C_m}{\partial C_L}\right)_w - \left(\frac{1}{C_{L_\alpha}} - \frac{d\epsilon}{dC_L}\right)\left(\frac{\partial C_L}{\partial \alpha}\right)_t \frac{q_t}{q}\frac{S_t}{S}\frac{l}{\bar{c}}$$

This approximate equation then qualitatively indicates that the principal components affecting the longitudinal stability (dC_m/dC_L) of the airplane are: (neglecting q_t/q)

1. $\left(\partial C_m/\partial C_L\right)_w$, static longitudinal stability of the wing–fuselage combination

2. $\partial C_L/\partial \alpha$, the lift–curve slope of the wing–fuselage combination

3. $d\epsilon/dC_L$, the rate of change of downwash at the tail with lift of the wing

4. $\left(\partial C_L/\partial \alpha\right)_t$, the lift–curve slope of the horizontal tail

Two lift ranges are considered in comparing these factors:

(a) The low lift range from a lift coefficient of −0.1 to 0.1, (measured at approximately $C_L = 0$)

(b) The high lift range from a lift coefficient of 0.2 to 0.3. (measured at approximately 0.3)

In order to illustrate the constant–speed static longitudinal stability characteristics of the XS–1 in the low lift range, as compared with the static longitudinal stability characteristics in the high lift range, figure 14 has been prepared. It may be noted that the model in the low lift range begins to become unstable at approximately a Mach number of 0.80, and the divergence between the stability at the two lift coefficients reaches a maximum at a Mach number of approximately 0.885.

The first component to be analyzed, the static longitudinal stability of the wing–fuselage combination, is shown in figure 15 and indicates a divergence for the two lift ranges considered between a Mach number of 0.825 and 0.9.

The lift–curve slope for the wing is shown in figure 16 for the two lift ranges considered. This figure indicates that the variation and trend with Mach number is essentially the same. The low–speed values are the same, the maximum value of the lift–curve slope occurs at a Mach number of about 0.80 for both lift ranges, and the lowest value of the lift–curve slope occurs at a Mach number of approximately 0.875. It should be noted that the magnitudes for the ranges considered are quite different, the low lift range producing the highest and the lowest values.

In considering the downwash component $(d\epsilon/dC_L)$ it may be noted in figure 17 that the variation and trend with Mach number are not the same for the two lift ranges considered, especially at high Mach numbers. The value of the $d\epsilon/dC_L$ is identical for both lift ranges at a Mach number of 0.70. However, in the low lift range the variation of downwash with lift coefficient increases rapidly with Mach number until

a value of 8.2 is reached at a Mach number of 0.875. This value is 142 percent greater than the value at a Mach number of 0.70. In the high lift range, on the other hand, the value of $d\epsilon/dC_L$ only decreases when a Mach number of 0.875 is reached. The trend is also divergent from a Mach number of 0.885 to 0.925.

The lift-curve slope of the horizontal tail as shown in figure 18 is the same for both lift ranges considered and therefore it has no effect on the difference in static longitudinal stability for the lift ranges considered.

This analysis illustrates qualitatively that the primary contributors to the instability of the XS-1 model at low lift coefficients and high Mach numbers are: (1) The longitudinal instability of the wing-fuselage combination, and (2) the increase in the rate of effective downwash with lift coefficient.

Figure 19 presents the stick-fixed neutral-point variation with Mach number when the model is in level flight at sea level and altitudes of 30,000 feet and 40,000 feet. An average rearward shift of the neutral point from 30-percent mean aerodynamic chord at a Mach number of 0.60 to 48-percent mean aerodynamic chord at a Mach number of 0.925 is shown for the altitude of 40,000 feet.

Control characteristics.- The variation of level-flight lift coefficient with Mach number for the model with a wing loading of 40 pounds per square foot at sea level and altitudes of 30,000 feet and 40,000 feet is presented in figure 20. The stabilizer settings and elevator deflections required to trim the model in level-flight at sea level and altitudes of 30,000 feet and 40,000 feet shown in figures 21 and 22 indicate a change of only a few degrees for either the stabilizer or elevator in the Mach number range between 0.825 and 0.925. It should be noted, however, that these changes, although not excessive, occur rapidly with small increase in Mach number and rapid manipulation of the control will be necessary.

The stabilizer and elevator effectiveness are shown in figures 23 and 24 for angles of attack of -2°, 0°, and 3°. The effectiveness of both stabilizer and elevator is practically the same for the angle-of-attack range tested. The stabilizer effectiveness decreases with increase in speed from a Mach number of 0.75 to 0.925.

The elevator effectiveness increases with speed until a Mach number of 0.825 is reached. Then a slight decrease is noted for angles of attack of 0° and 3°. The decrease is slightly more rapid for an angle of attack of -2° up to the highest test Mach number of 0.925.

In the figures just presented for stabilizer and elevator effectiveness, the effect of downwash and dynamic pressure at the tail

is included. However, in figure 25 the effectiveness of the horizontal tail without downwash effects is shown with Mach number and indicates the effects of compressiblity and fuselage interference on the horizontal tail.

CONCLUSIONS

1. A drag force break occurs at a Mach number of 0.78, followed by a rapid rise in drag coefficient with Mach number for a lift coefficient of 0.1.

2. A lift force break occurs at a Mach number of 0.80, followed by a decrease and then an increase in lift coefficient with Mach number for an angle of attack of 0°.

3. This configuration has a high degree of constant-speed static longitudinal stability except for a narrow range of Mach number (approximately 0.875 to 0.90) at low lift coefficients.

4. Stabilizer and elevator effectiveness tend to decrease at the high Mach numbers, but no serious control problems are expected up to the highest Mach number investigated because the lowest degree of effectiveness is still of such a magnitude as to control changes in trim for level flight at the desired altitudes.

5. Tuft surveys of the aft portion of the fuselage showed no separation or unusual flow patterns up to a Mach number of 0.925 for a maximum angle of attack of 3° and a maximum yaw angle of 2.2°.

6. The results show that the speed-retarding brakes located on the fuselage behind the wing are barely capable of reducing the terminal velocity of the airplane to the critical Mach number range.

Langley Memorial Aeronautical Laboratory
National Advisory Committee for Aeronautics
Langley Field, Va.

REFERENCES

1. Mattson, Axel T.: Force and Longitudinal Control Characteristics of a $\frac{1}{16}$-Scale Model of the Bell XS-1 Transonic Research Airplane at High Mach Numbers. NACA RM No. L7A03, 1947.

2. Byrne, Robert W.: Experimental Constriction Effects in High-Speed Wind Tunnels. NACA ACR No. L4L07a, 1944.

3. Glauert, H.: Wind Tunnel Interference on Wings, Bodies and Airscrews. R. & M. No. 1566, British A.R.C., 1933.

4. Thom, A.: Blockage Corrections and Choking in the R.A.E. High Speed Tunnel. Rep. No. Aero 1891, British R.A.E., Nov. 1943.

5. Goldstein, S., and Young, A. D.: The Linear Perturbation Theory of Compressible Flow, with Applications to Wind-Tunnel Interference. R. & M. No. 1909, British A.R.C., 1943.

TABLE I.- PHYSICAL CHARACTERISTICS OF THE BELL

XS-1 TRANSONIC RESEARCH AIRPLANE

Power:	
Four rocket units, each capable of delivering 1500 pounds thrust, grouped in rear of fuselage	
Wing loading:	
Take-off, lb/sq ft	103
Landing, lb/sq ft	40
Wing:	
Area, sq ft	130
Span, ft	28
Mean aerodynamic chord, in	57.1
Aspect ratio	6
Root and tip sections	65,-110 (a = 1.0)
Incidence (root chord to thrust line)	2.5
Incidence (tip chord to thrust line)	1.5
Horizontal tail:	
Total area, sq ft	26.0
Span, ft	11.4
Aspect ratio	5
Root-mean-square-chord of elevator, ft	0.464
Root and tip sections	65-008

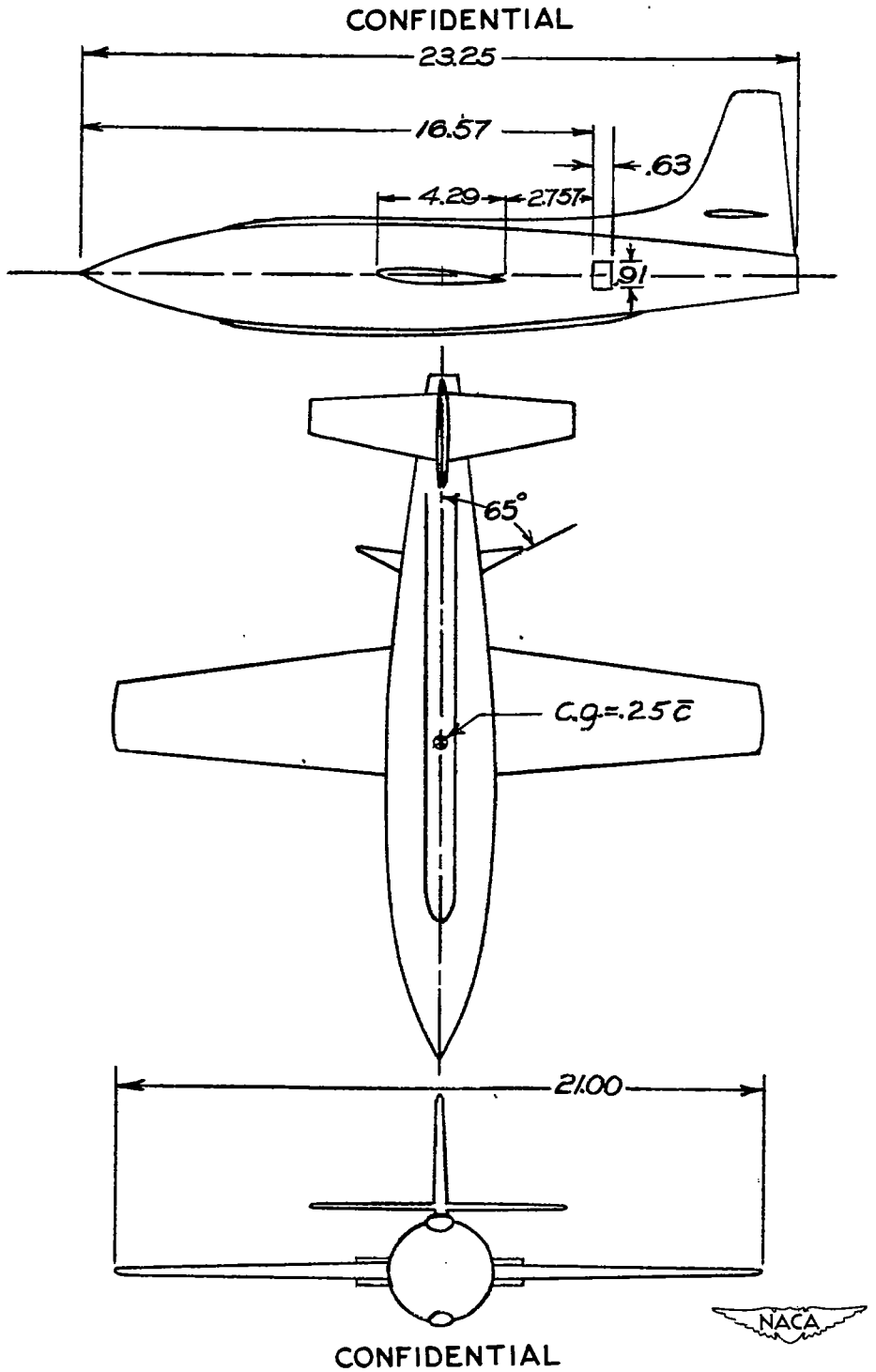

Figure 1.— Three-view drawing of a 1/16-scale model of the Bell XS-1 airplane with speed-reduction brakes as tested in the Langley 8-foot high-speed tunnel. All dimensions in inches.

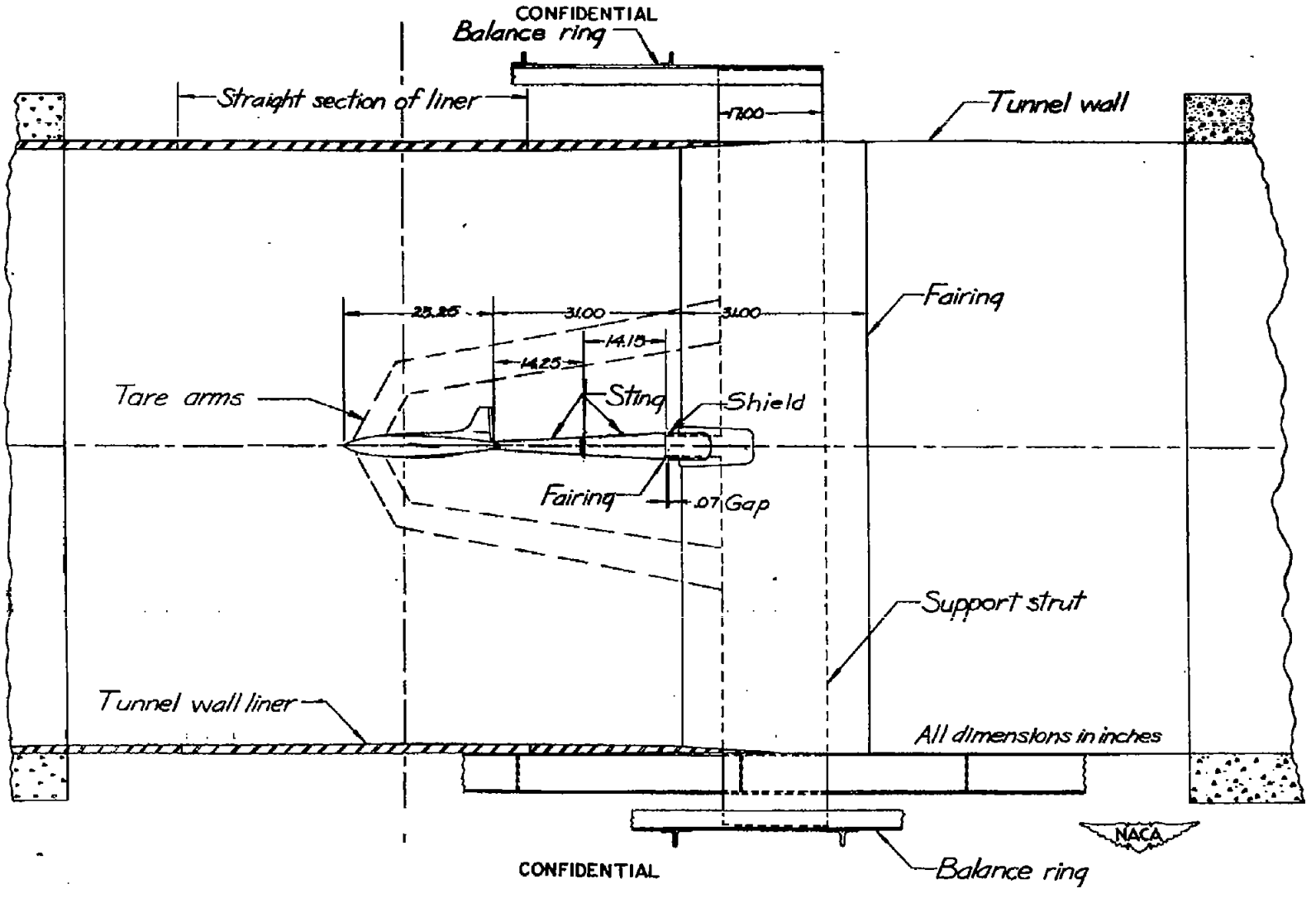

Figure 2.– XS-1 model on sting support in the Langley 8-foot high-speed tunnel.

CONFIDENTIAL

Run		Balance ring measures
Normal, N	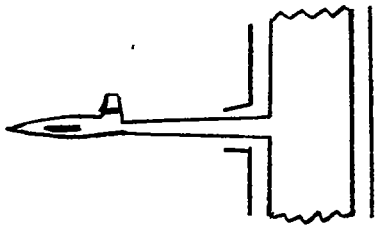	Model force Sting force Interference of sting on model Interference of model on sting Internal force
Tare A	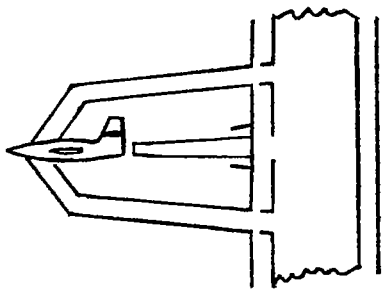	Model force Tare-arm force Guy-wire force Interference of model on arms Interference of sting on model Interference of arms on model
Tare B	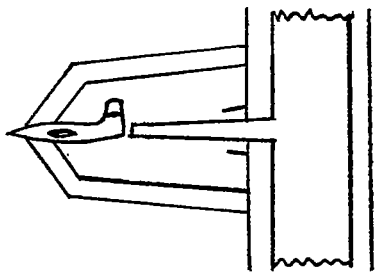	Sting force Interference of model on sting Interference of tare arms on sting Internal force
Tare C	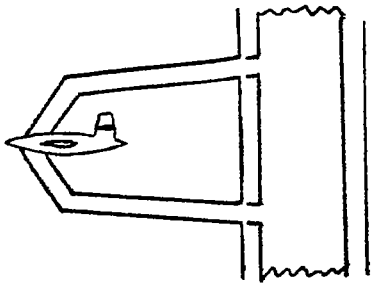	Model force Tare-arm force Guy-wire force Interference of model on arms Interference of arms on model

NACA

$$\text{Model force} = \text{normal run N} - \left[\text{Tare run B} + (\text{tare run A} - \text{tare run C})\right]$$

Figure 3 .-Methods employed in the Langley 8-foot high-speed tunnel for obtaining corrected model-force data on the Bell XS-1 transonic research airplane.

CONFIDENTIAL

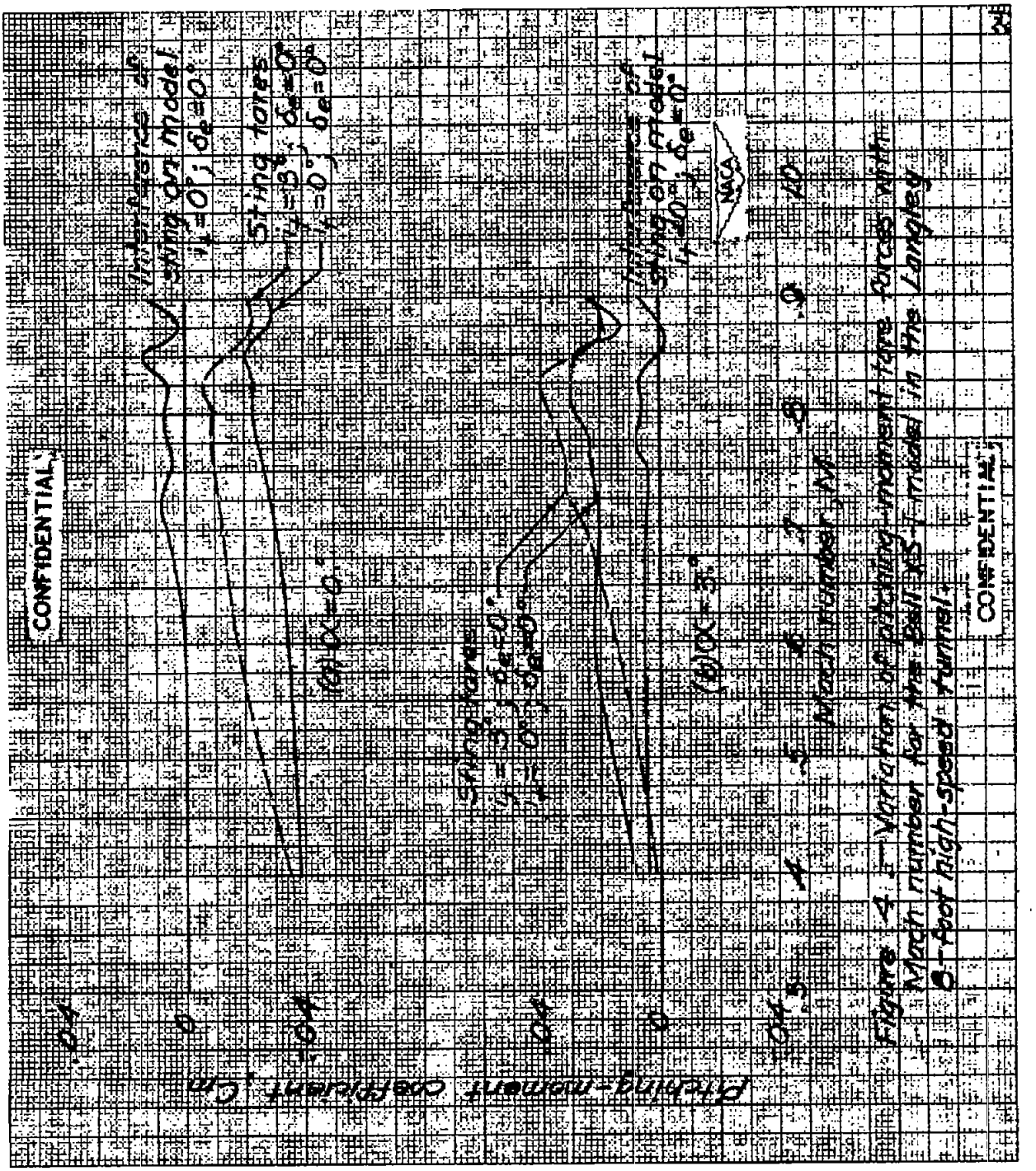

Figure 4.- Variation of pitching-moment coefficient with Mach number for the Bell XS-1 model in the Langley 8-foot high-speed tunnel.

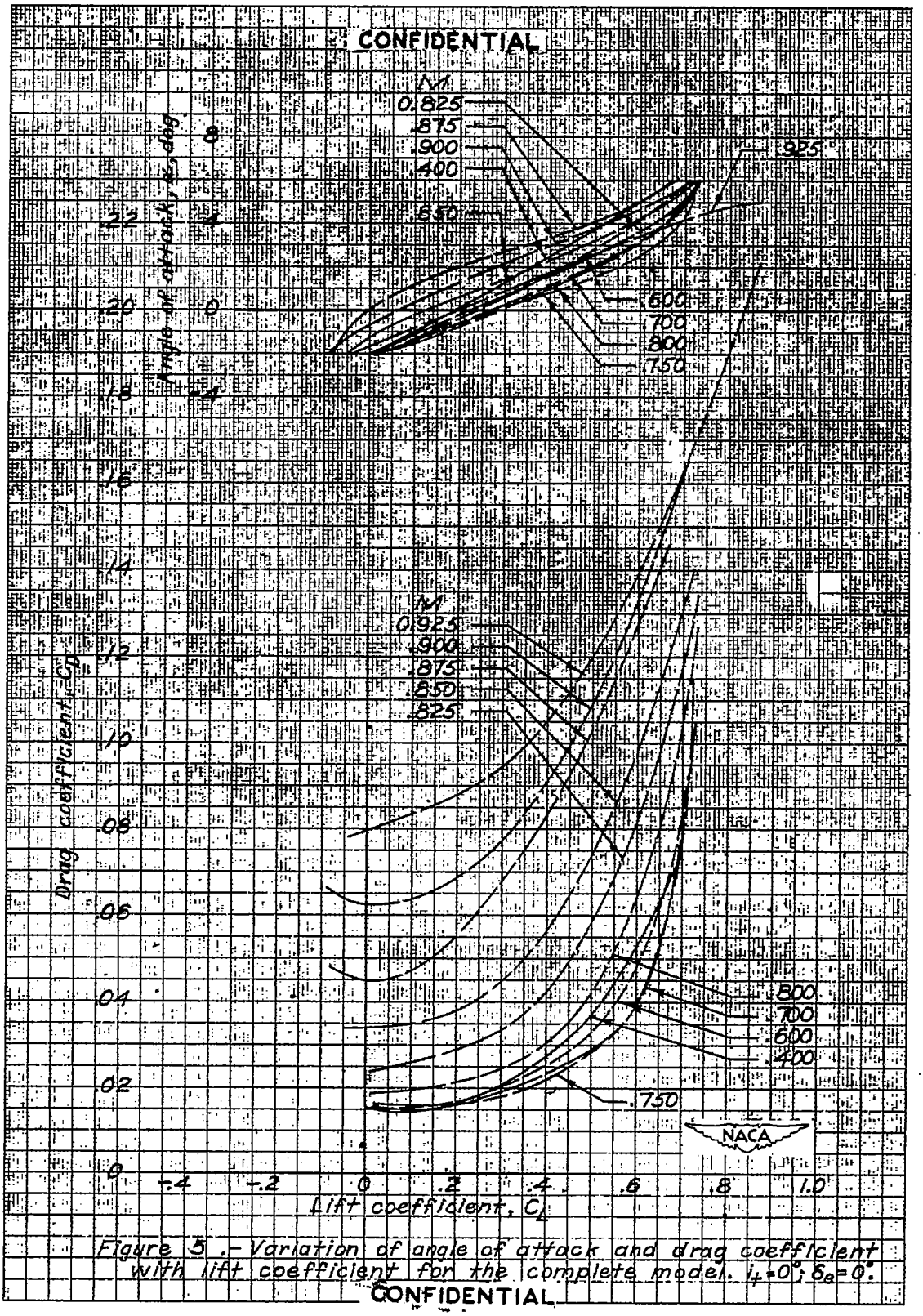

Figure 5.- Variation of angle of attack and drag coefficient with lift coefficient for the complete model. $i_t=0°$; $\delta_e=0°$.

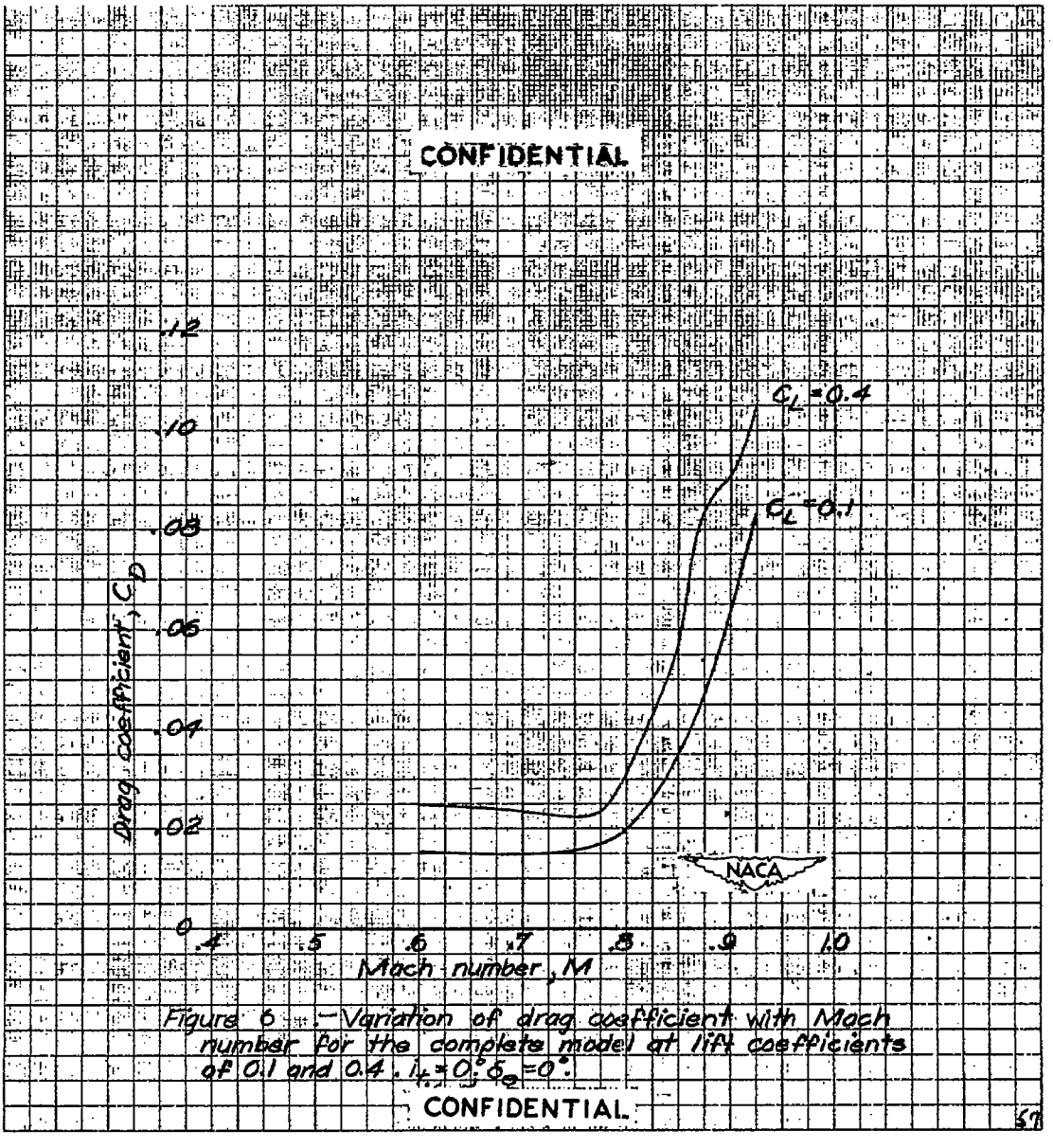

Figure 6.—Variation of drag coefficient with Mach number for the complete model at lift coefficients of 0.1 and 0.4. $i_t = 0°$; $\delta_e = 0°$.

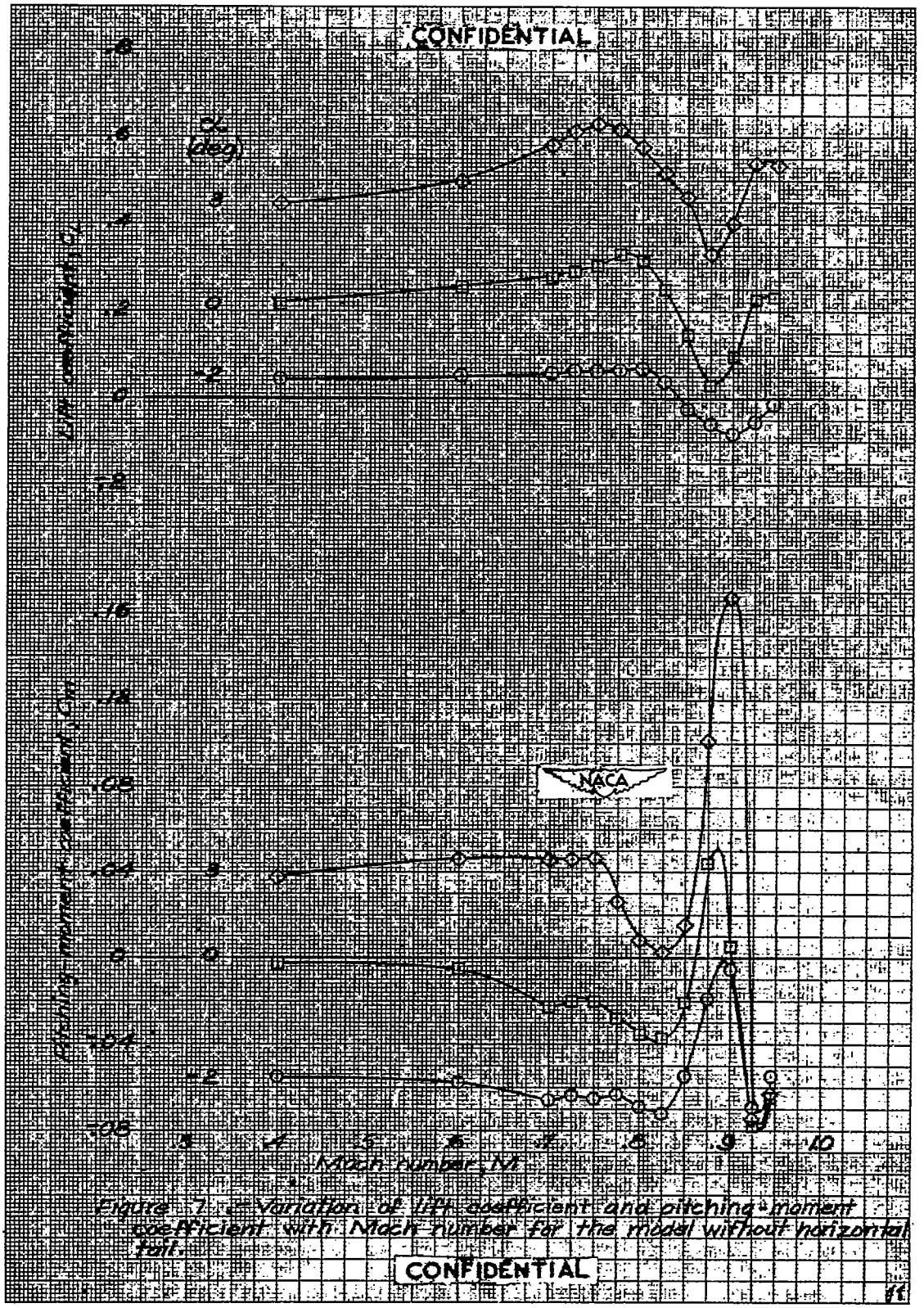

Figure 7.- Variation of lift coefficient and pitching-moment coefficient with Mach number for the model without horizontal tail.

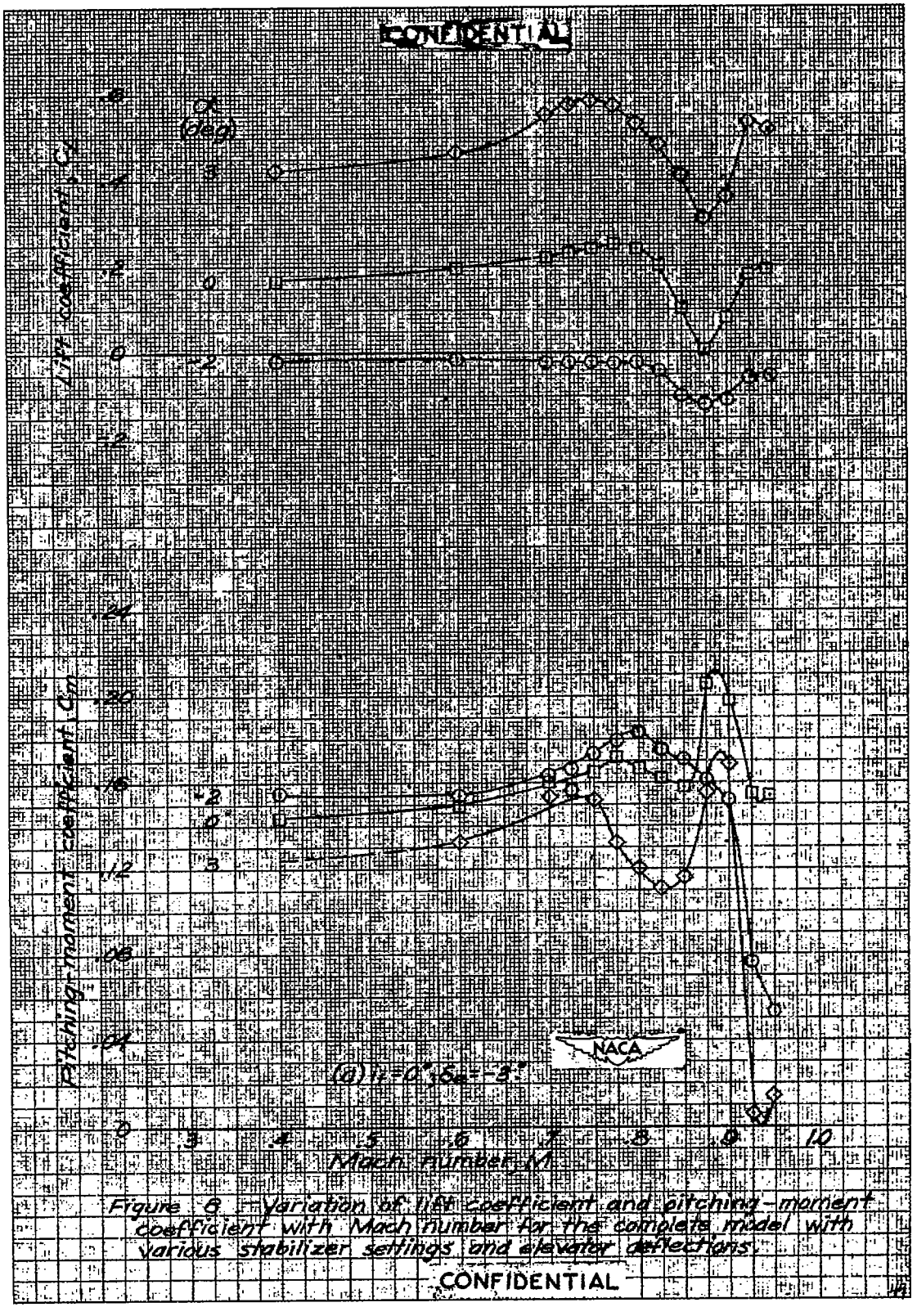

Figure 9.- Variation of lift coefficient and pitching-moment coefficient with Mach number for the complete model with various stabilizer settings and elevator deflections.

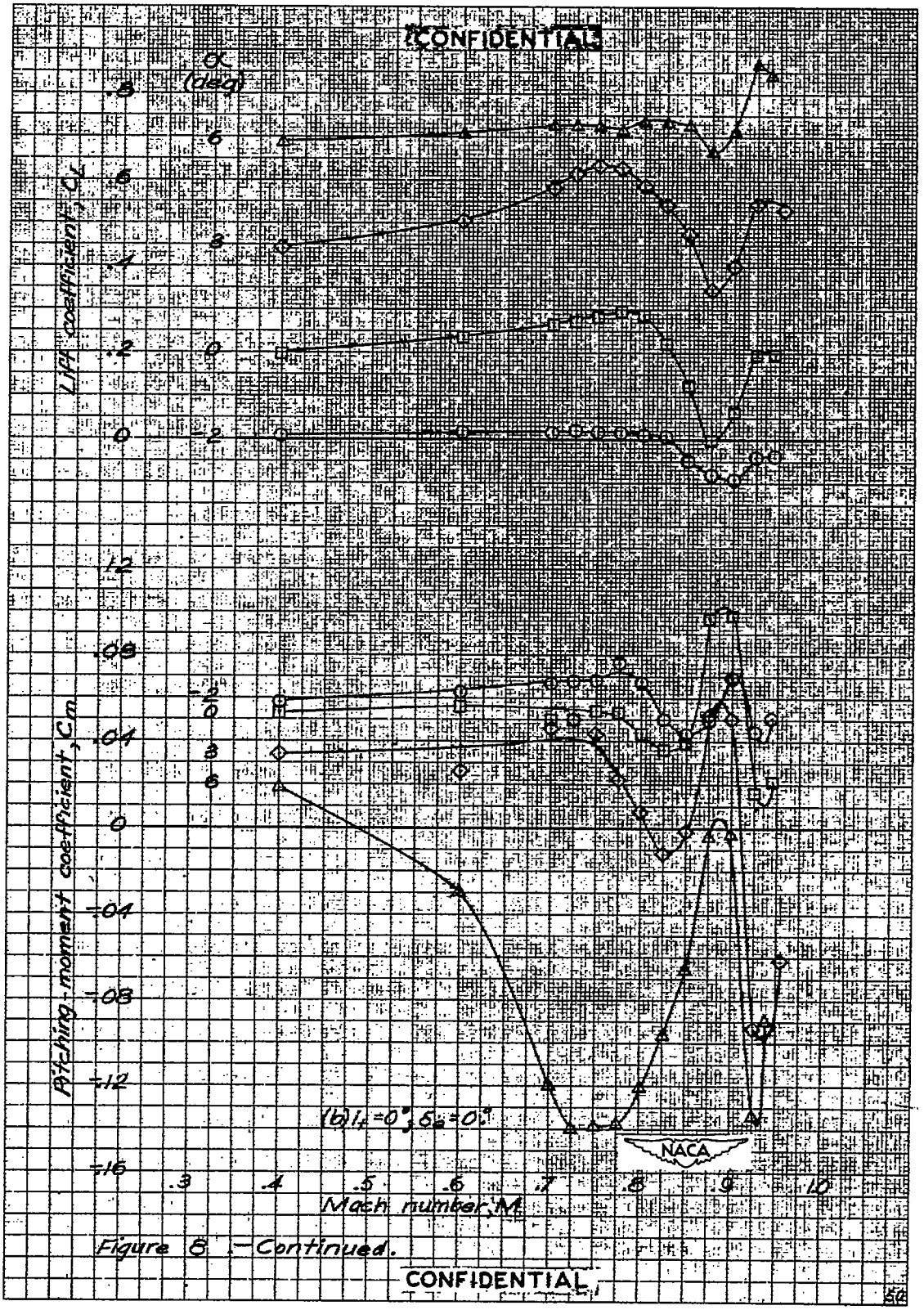

Figure 8.- Continued.

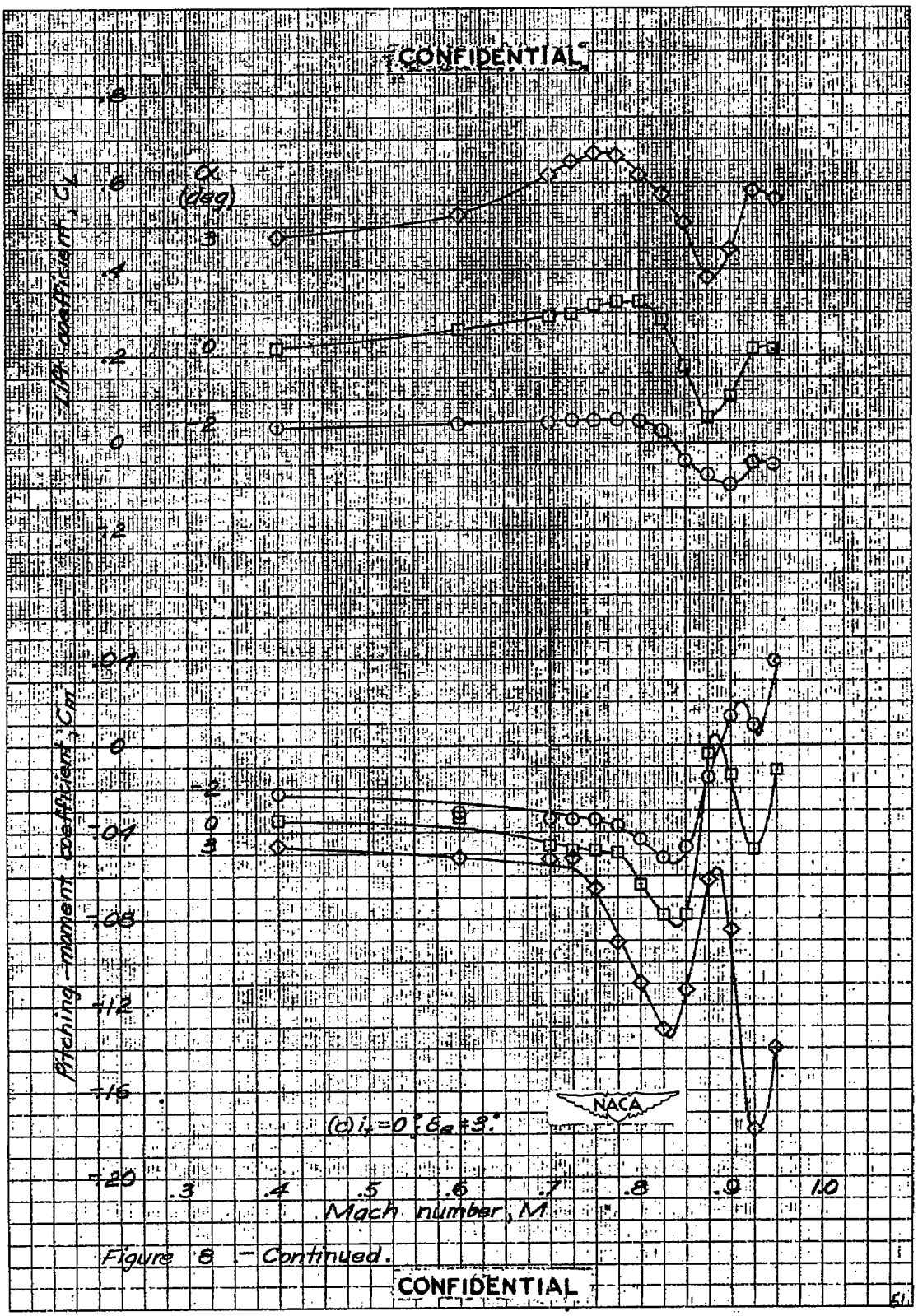

Figure 8.- Continued.

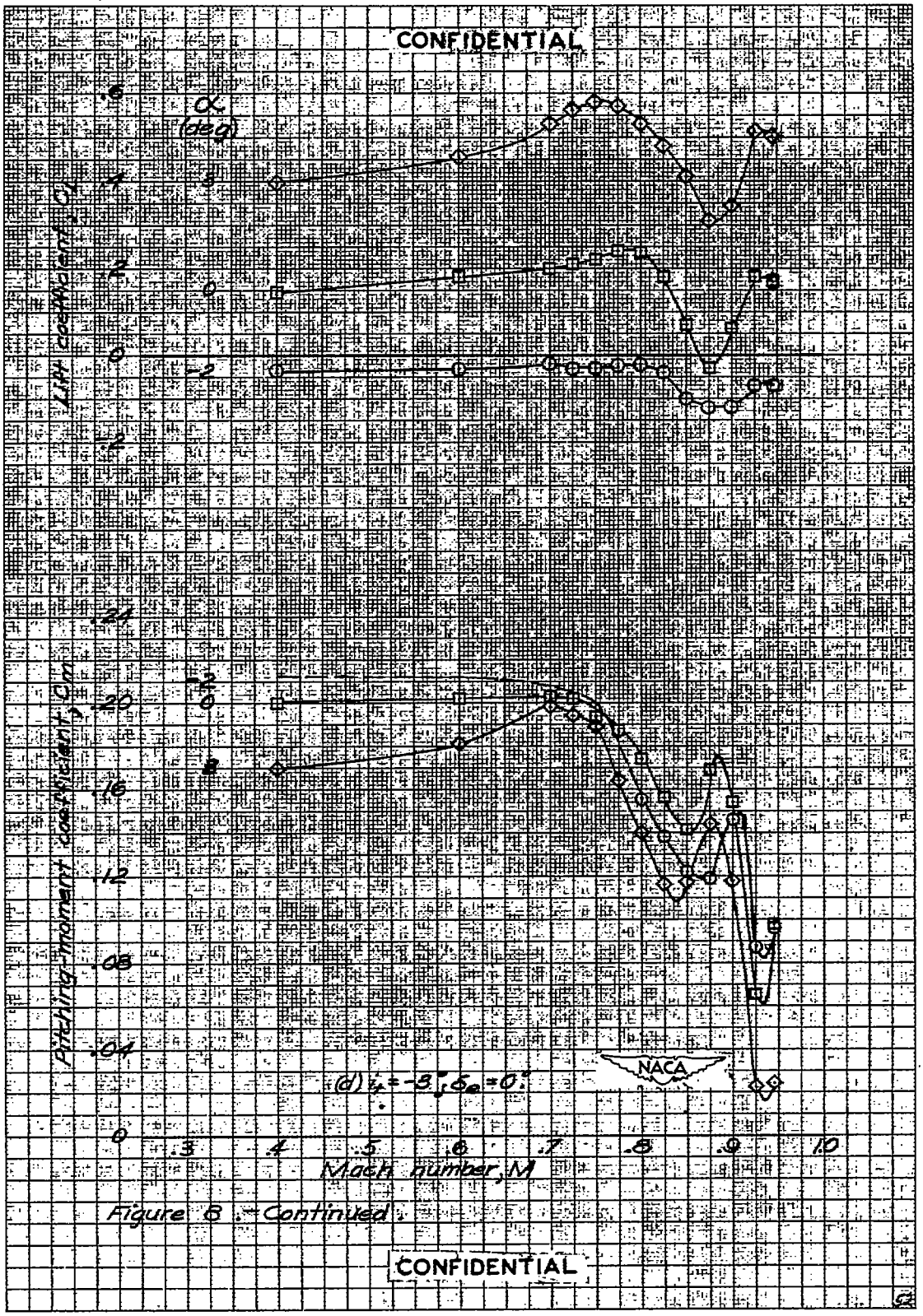

Figure 8.- Continued.

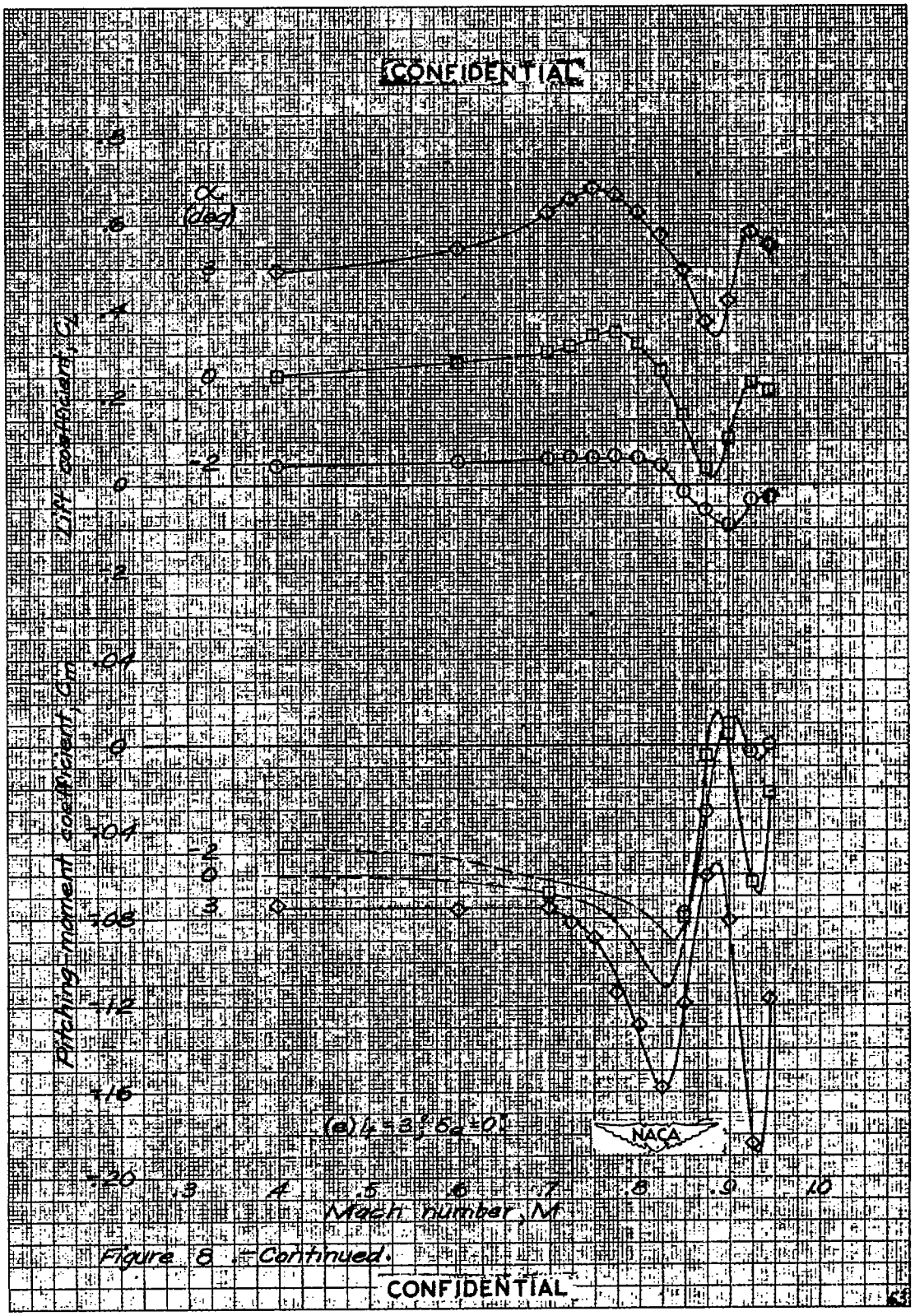

Figure 8.- Continued.

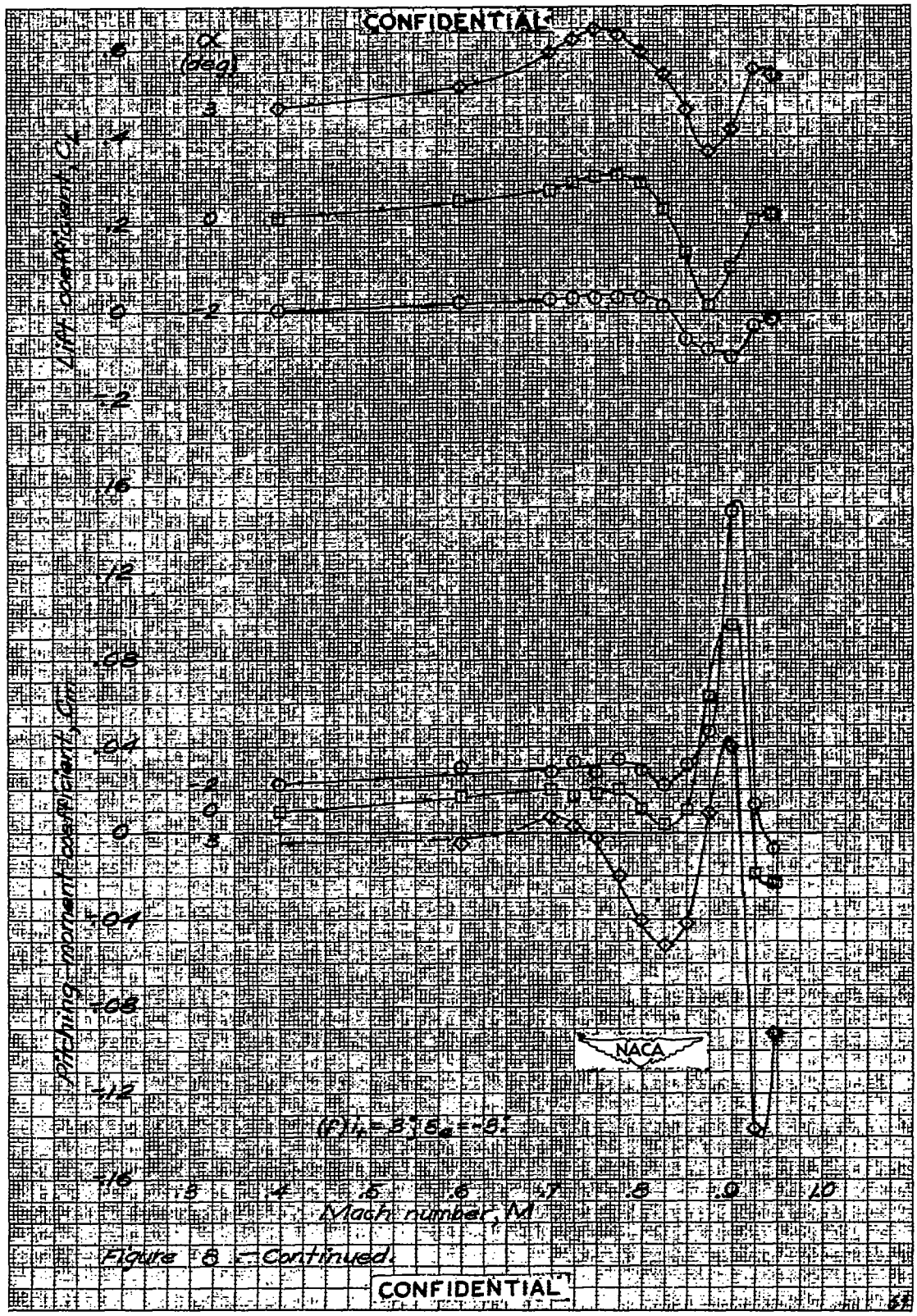

Figure 8 - Continued.

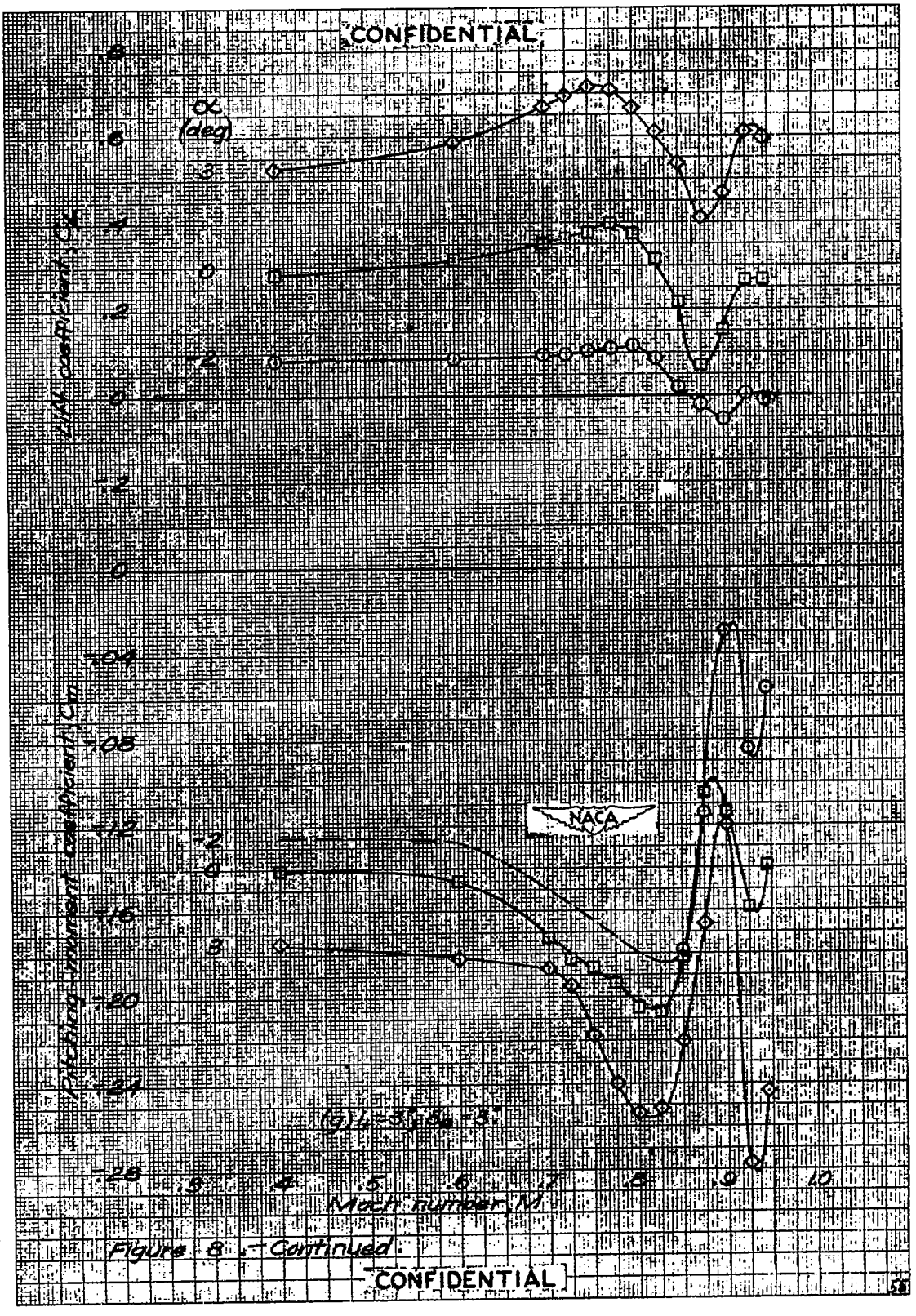

Figure 8.- Continued.

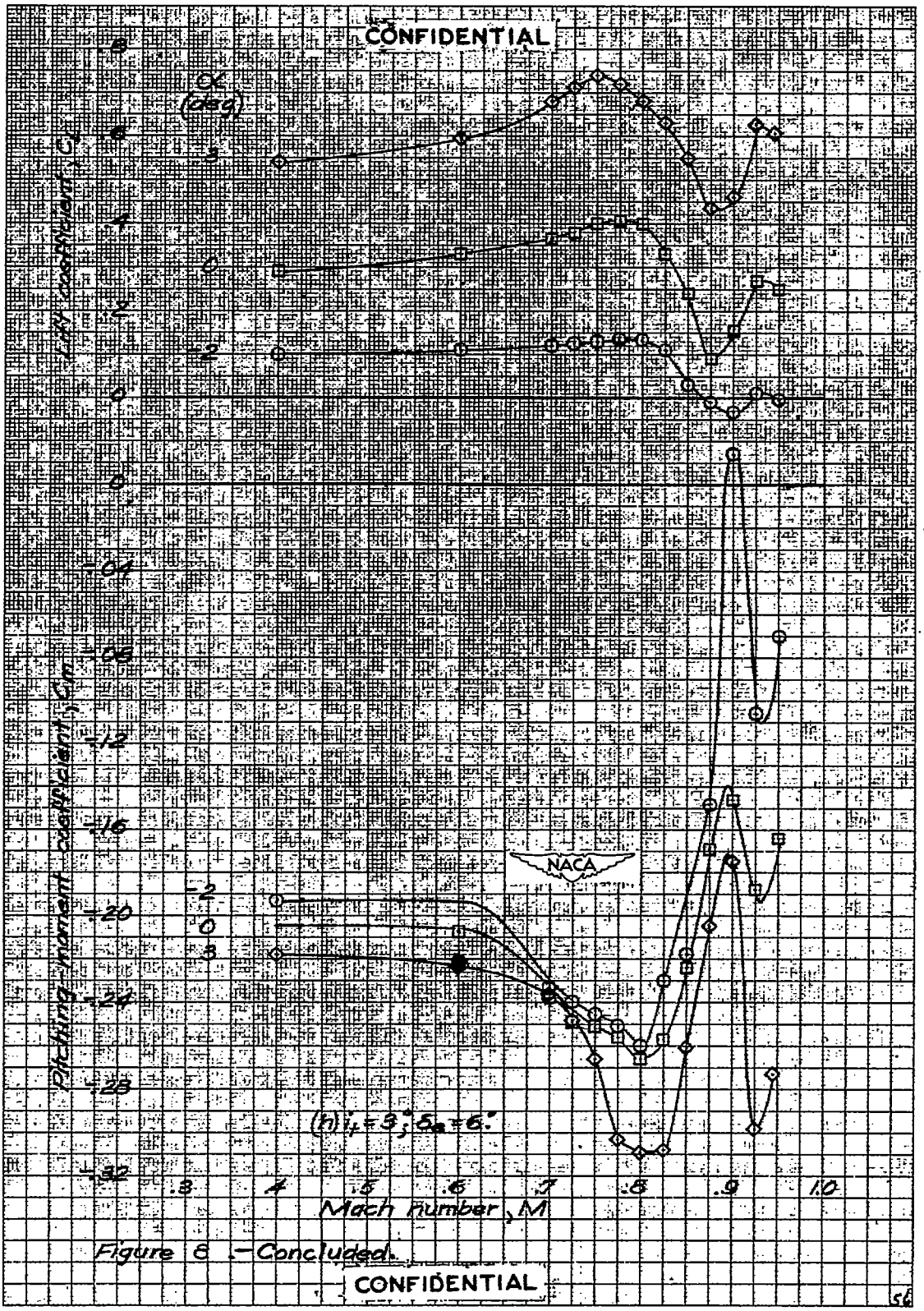

Figure 8.—Concluded.

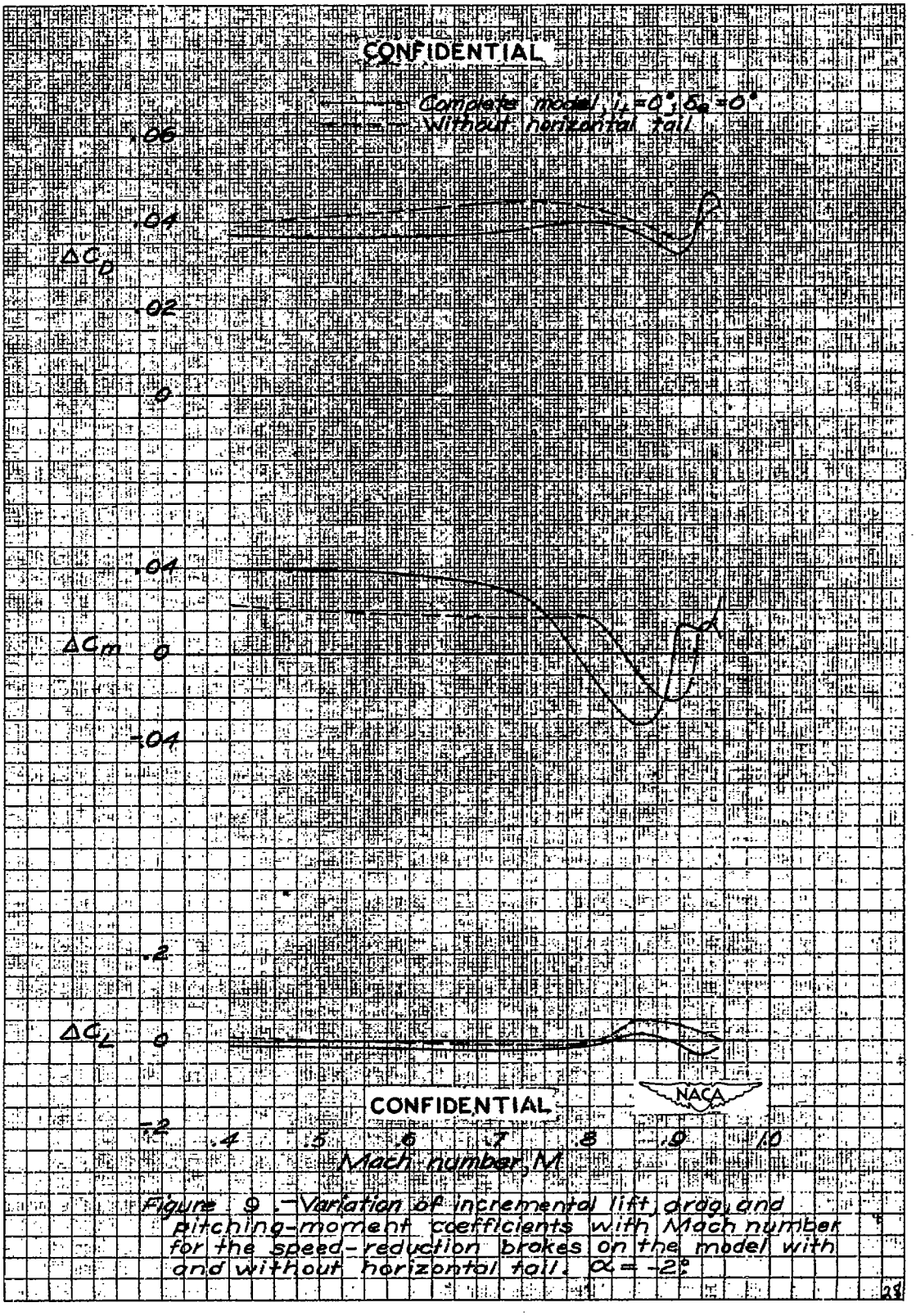

Figure 9.—Variation of incremental lift, drag, and pitching-moment coefficients with Mach number for the speed-reduction brakes on the model with and without horizontal tail. $\alpha = -2°$.

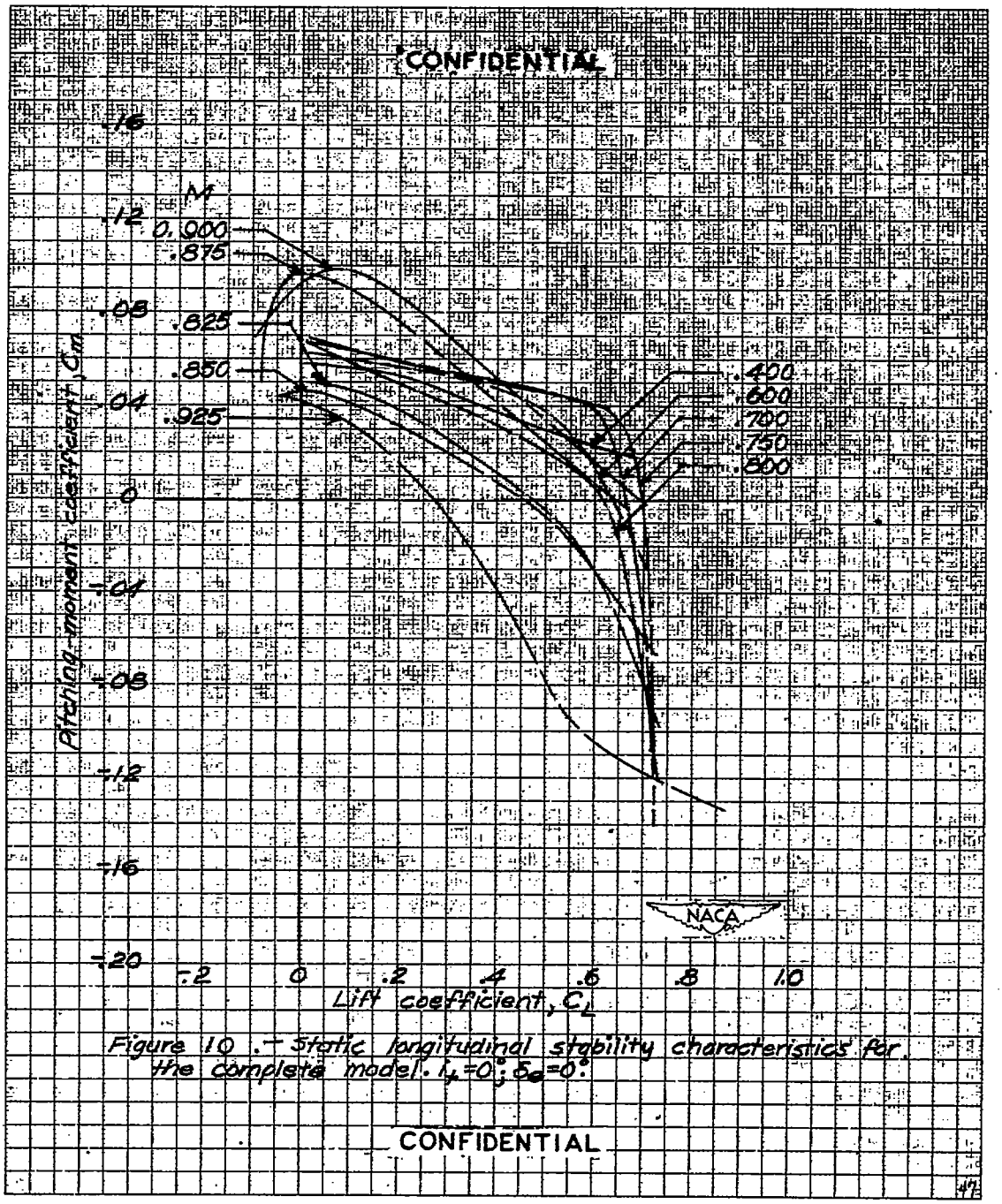

Figure 10.- Static longitudinal stability characteristics for the complete model. $i_t=0°$; $\delta_e=0°$.

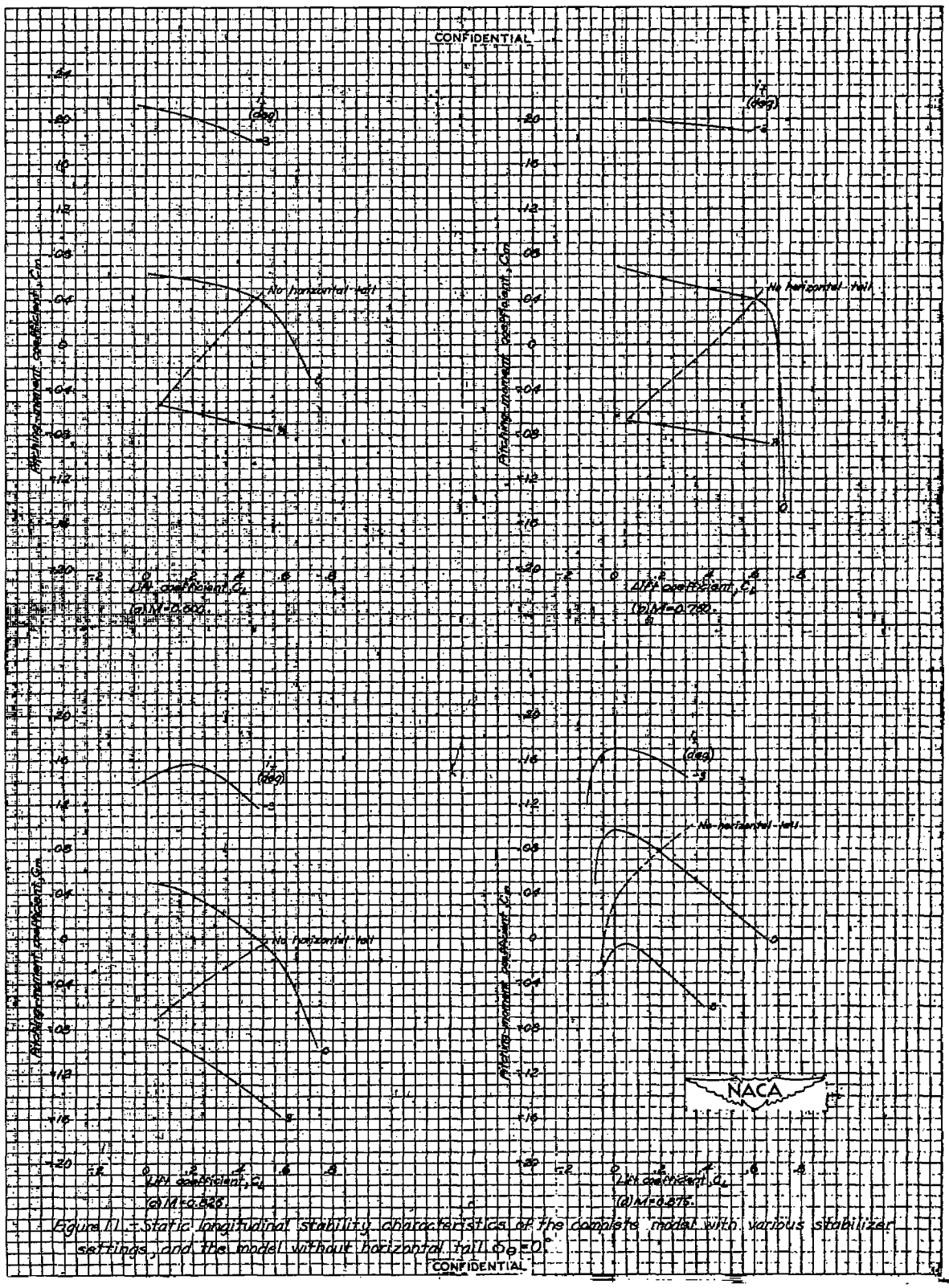

Figure 11.- Static longitudinal stability characteristics of the complete model with various stabilizer settings, and the model without horizontal tail $\delta_s=0°$.

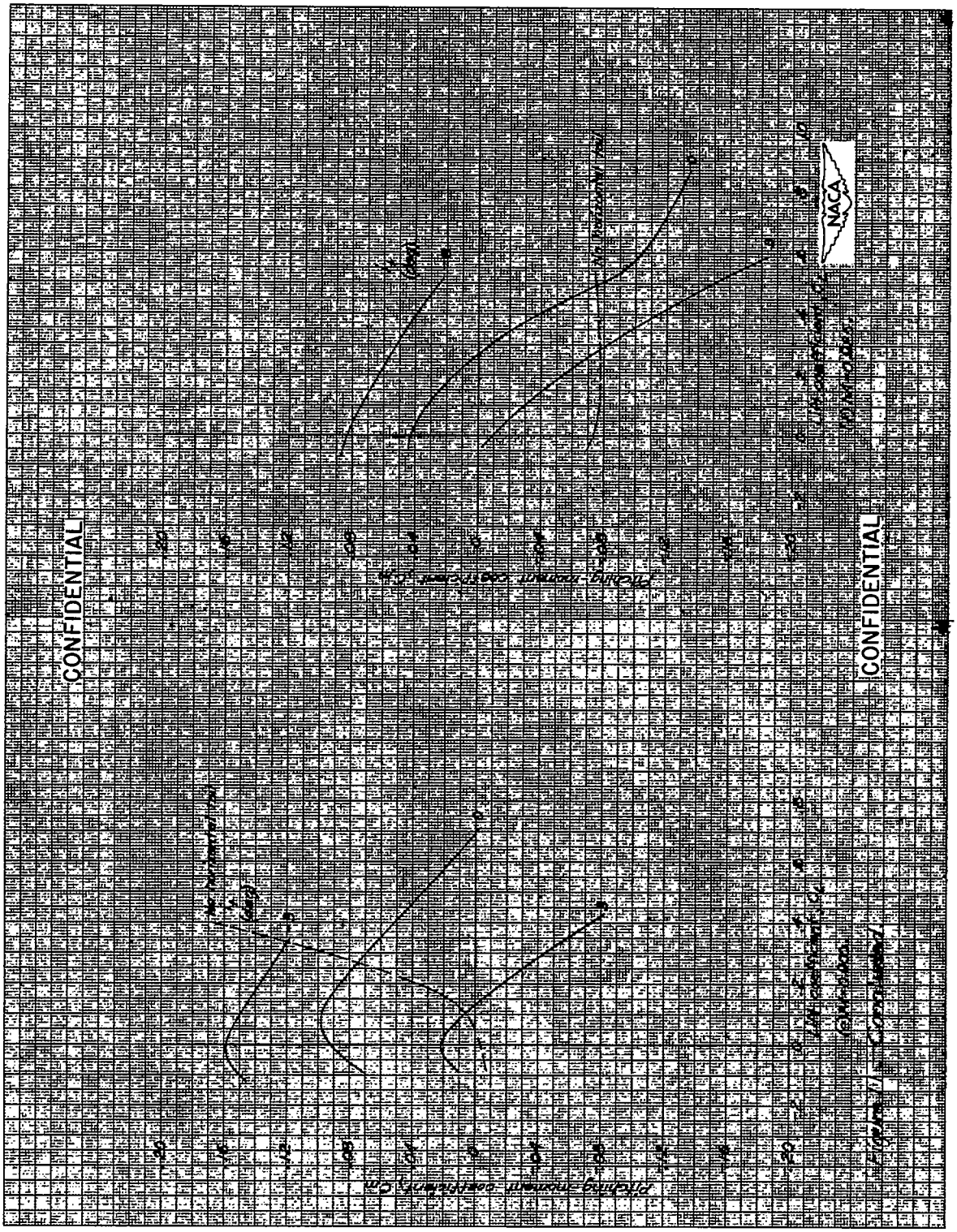
CONFIDENTIAL
CONFIDENTIAL
NACA

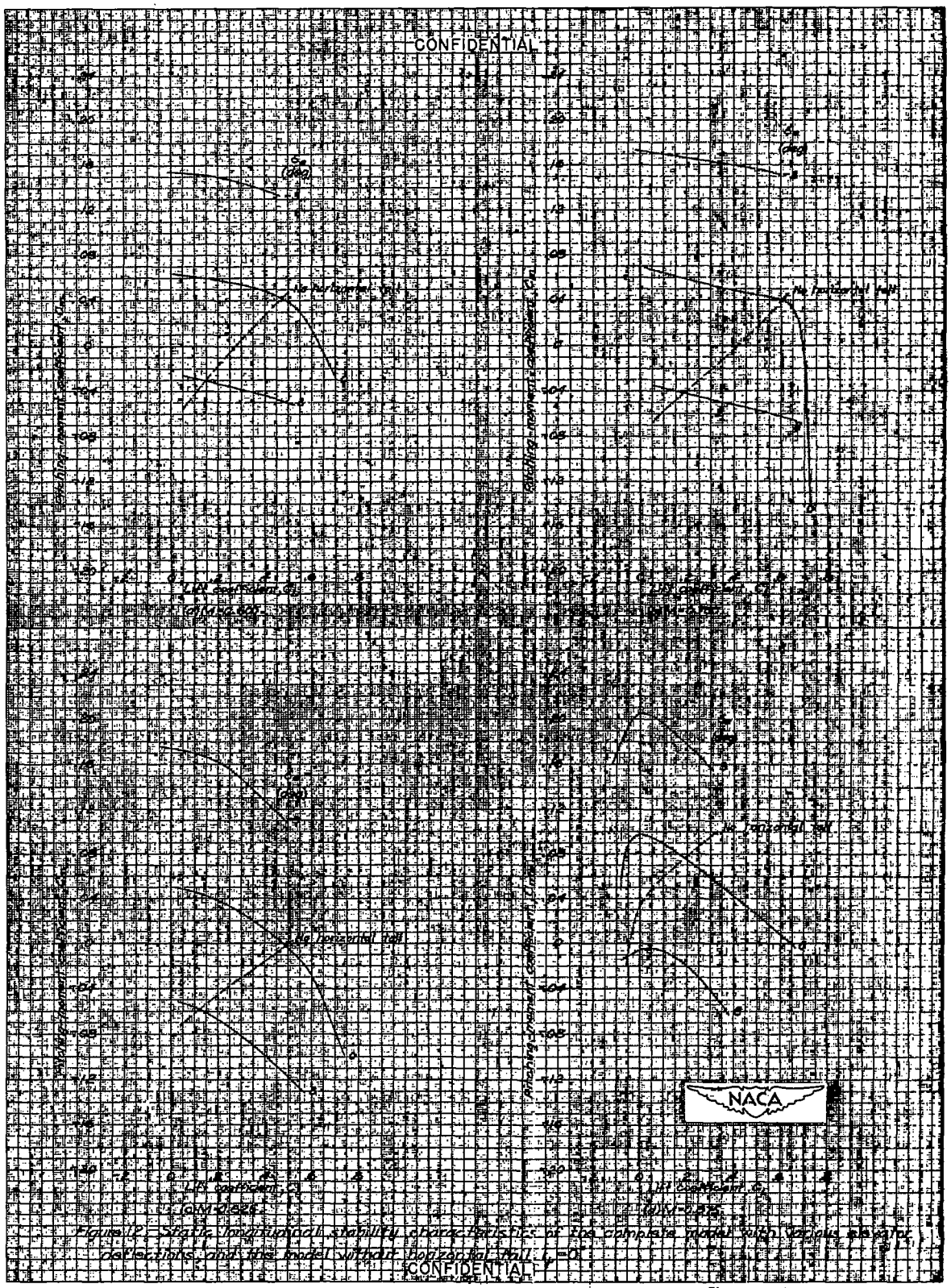

Figure 12.- Static longitudinal stability characteristics of the complete model with various elevator deflections, and the model without horizontal tail. $i_t = 0°$.

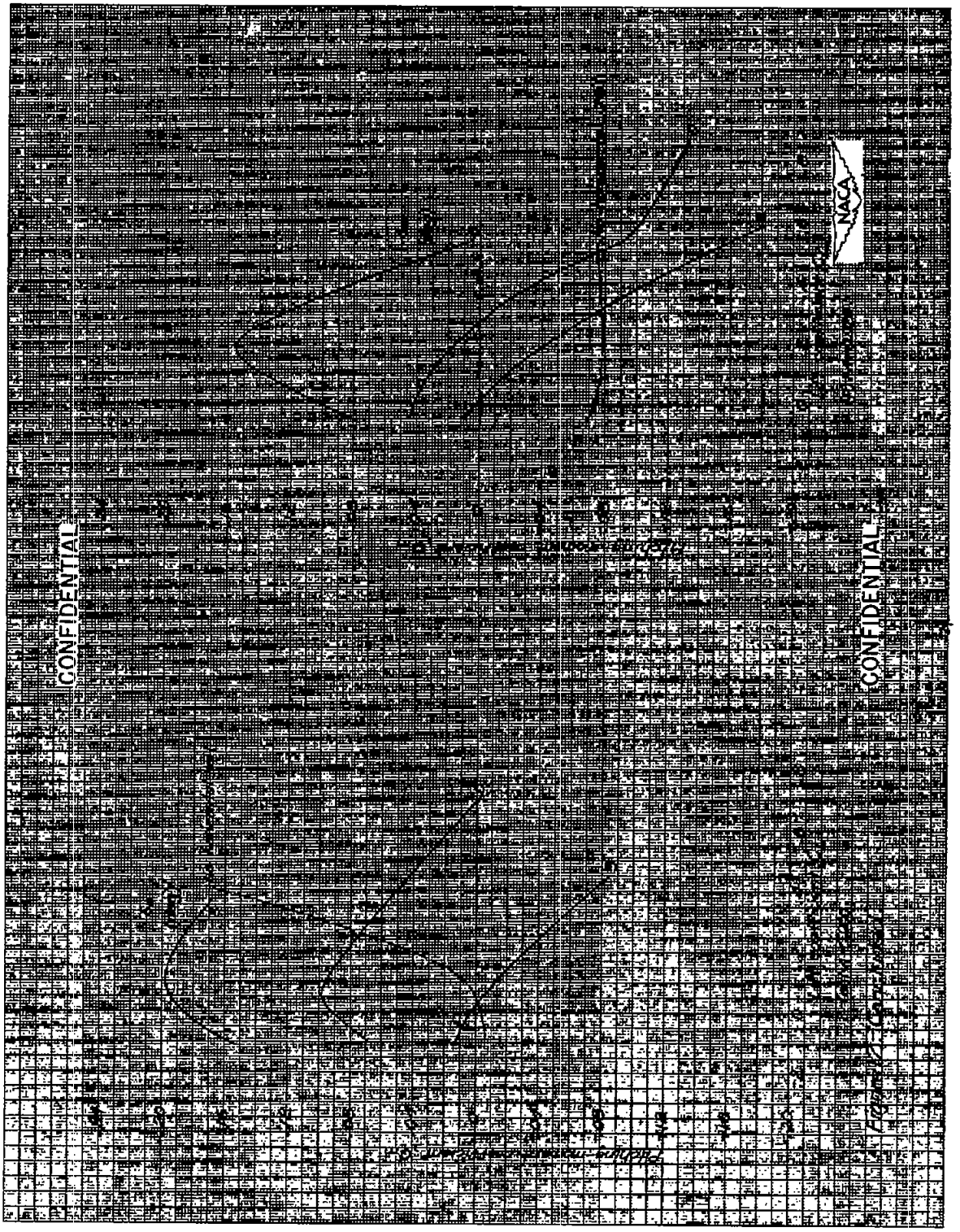
CONFIDENTIAL
CONFIDENTIAL
NACA

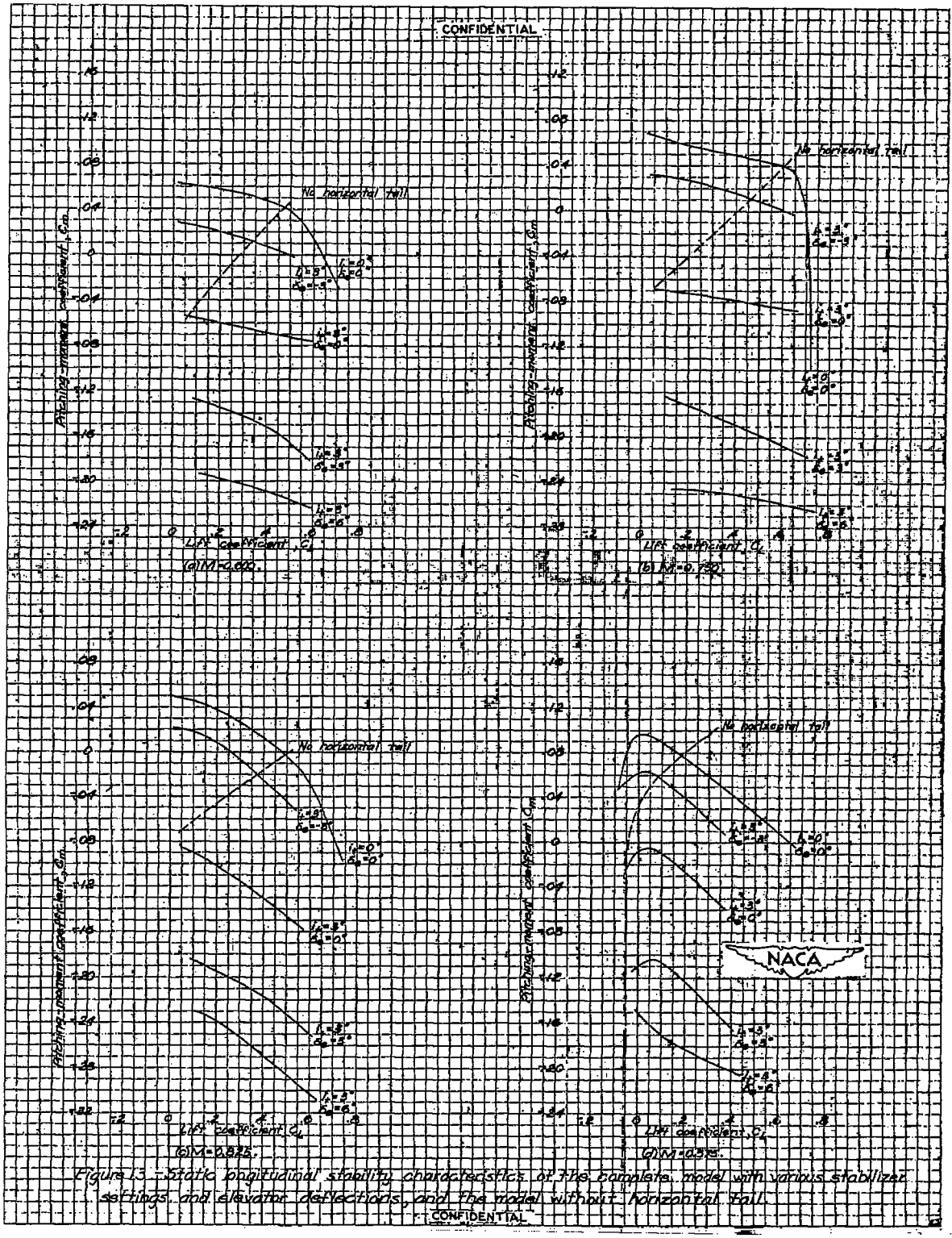

Figure 13.- Static longitudinal stability characteristics of the complete model with various stabilizer settings and elevator deflections, and the model without horizontal tail.

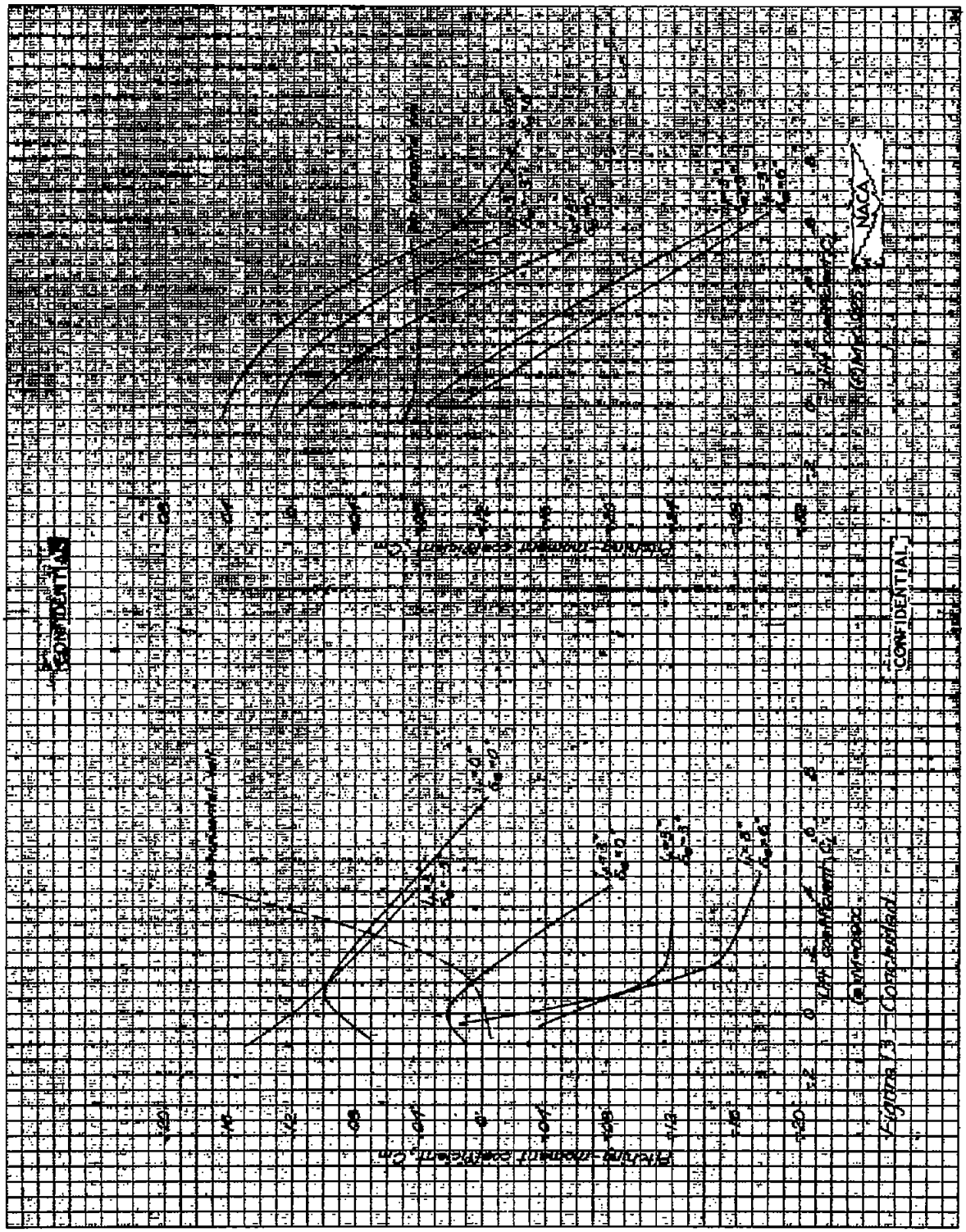

Figure 13.—Concluded.

Figure 13.- Concluded.

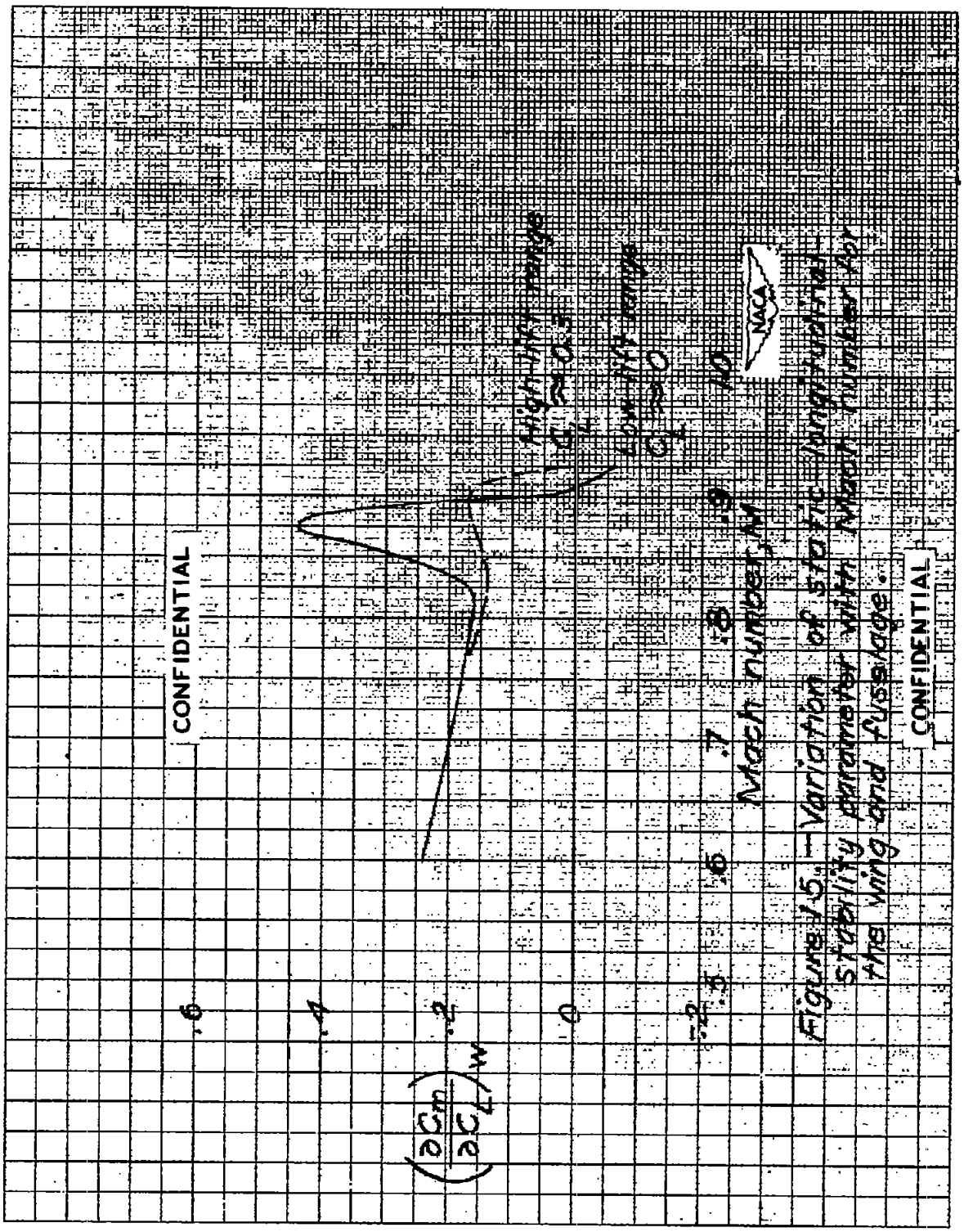

Figure 15.- Variation of static longitudinal stability parameter with Mach number for the wing and fuselage.

Figure 16.- Variation of lift-curve slope of the wing and fuselage with Mach number for the low-lift and high-lift ranges.

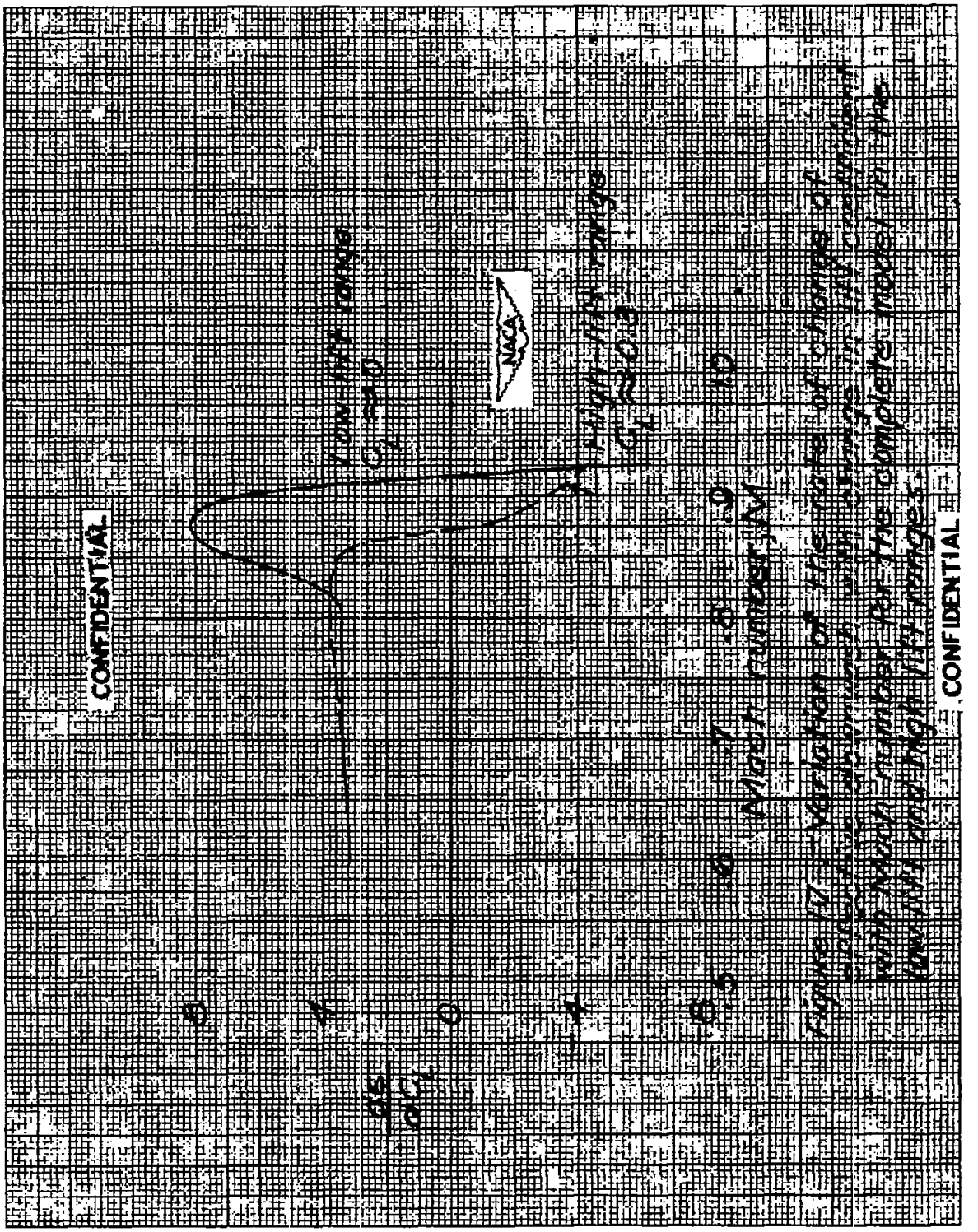
CONFIDENTIAL
NACA
CONFIDENTIAL

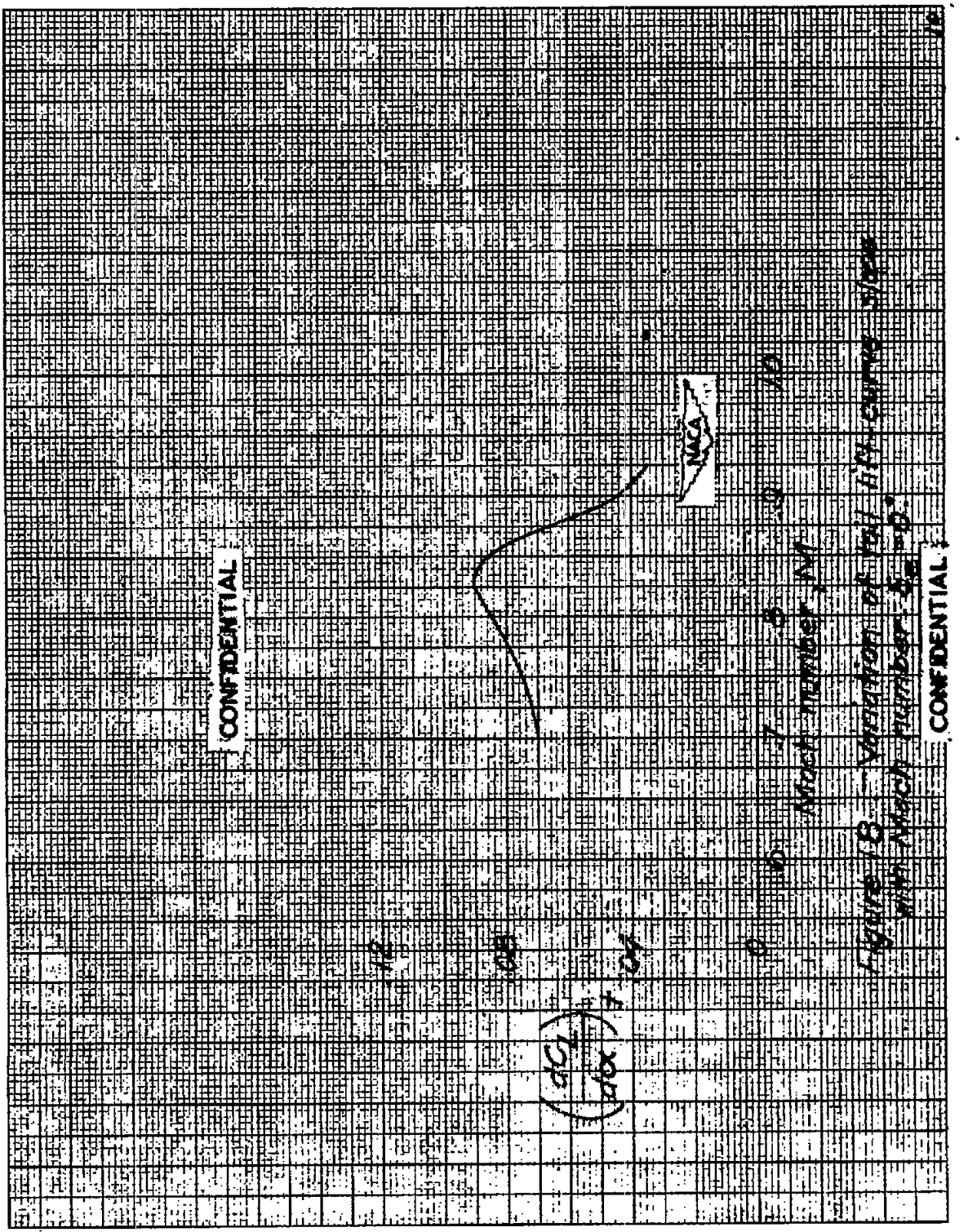

Figure 13.- Variation of $\left(\frac{dC_m}{dC_L}\right)_{C_L=0}$ with Mach number.

Figure 19.- Variation of neutral-point location, in percent M.A.C., with Mach number for the complete model in level flight at altitudes of 30,000 feet, 40,000 feet, and sea level. Wing loading, 40 pounds per square foot.

Figure 20.—Variation of level-flight lift coefficient with Mach number for a wing loading of 40 pounds per square foot at altitudes of 30,000 feet, 40,000 feet, and sea level.

Figure 21.- Variation of stabilizer setting for trim with Mach number for level flight at altitudes of sea level, 30,000 feet, and 40,000 feet. $\delta_e = 0°$.

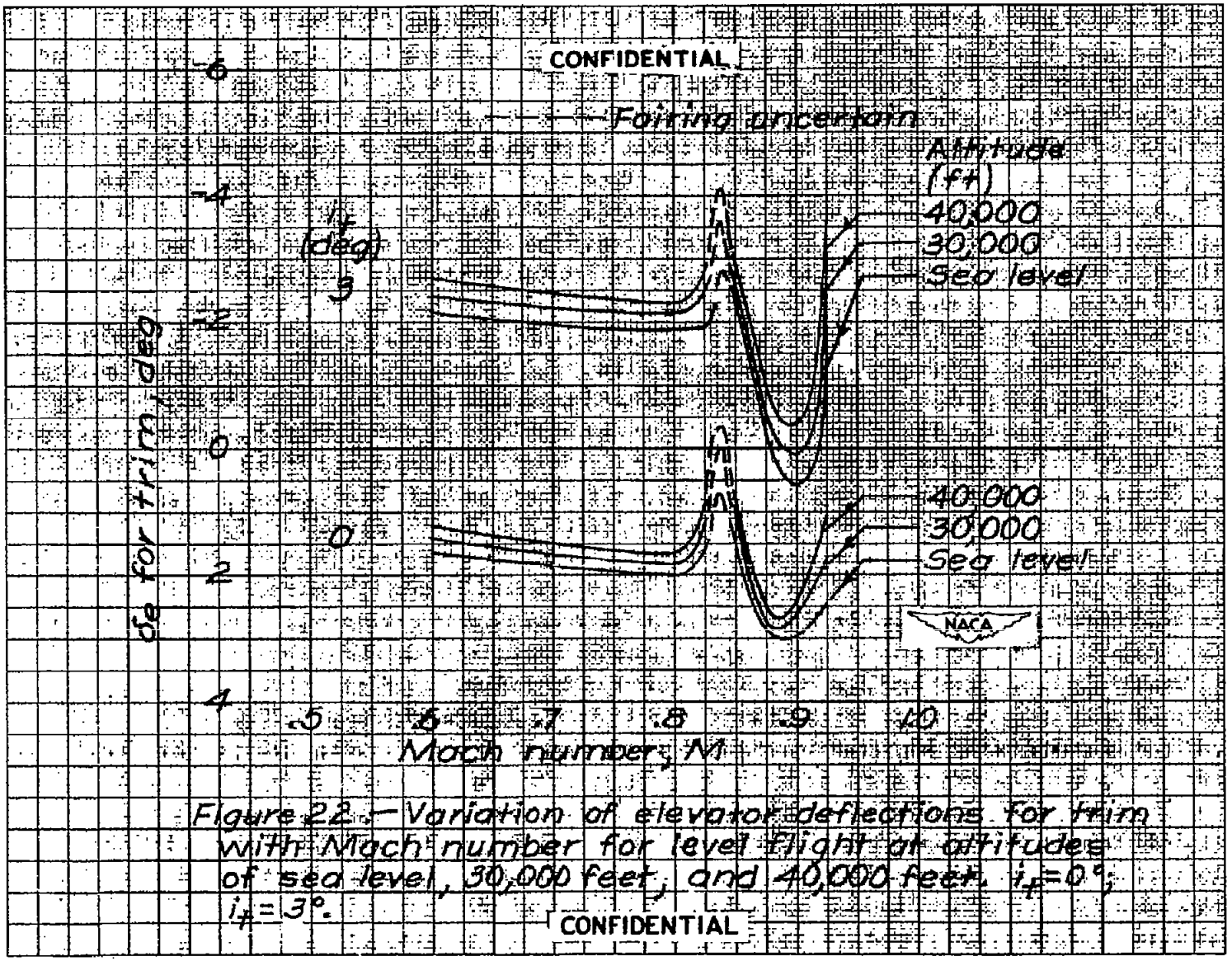

Figure 22.- Variation of elevator deflections for trim with Mach number for level flight at altitudes of sea level, 30,000 feet, and 40,000 feet. $i_t = 0°$; $i_t = 3°$.

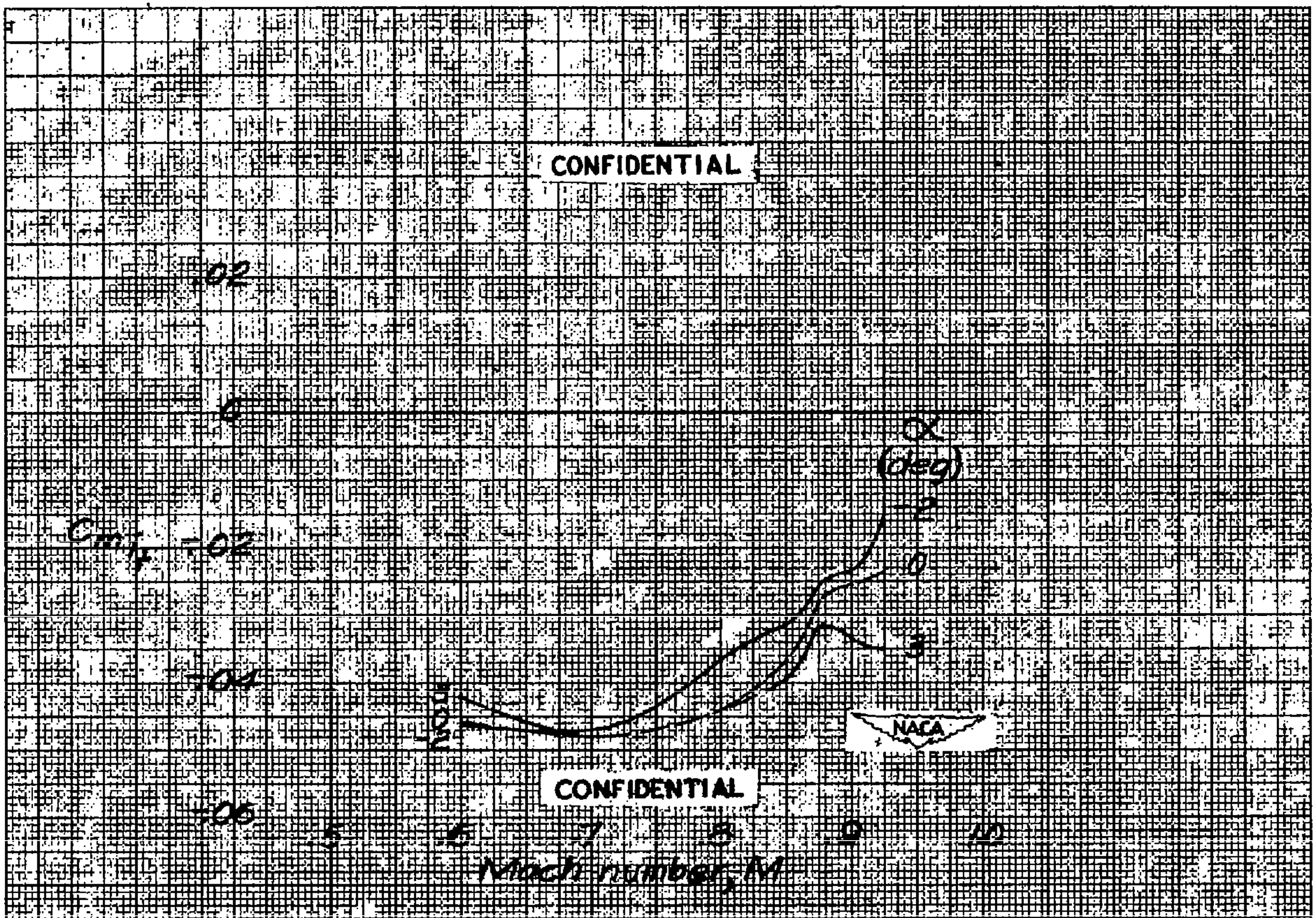

Figure 25. – Variation of stabilizer effectiveness with Mach number. $\delta_e = 0°$, $i_t = 0°$.

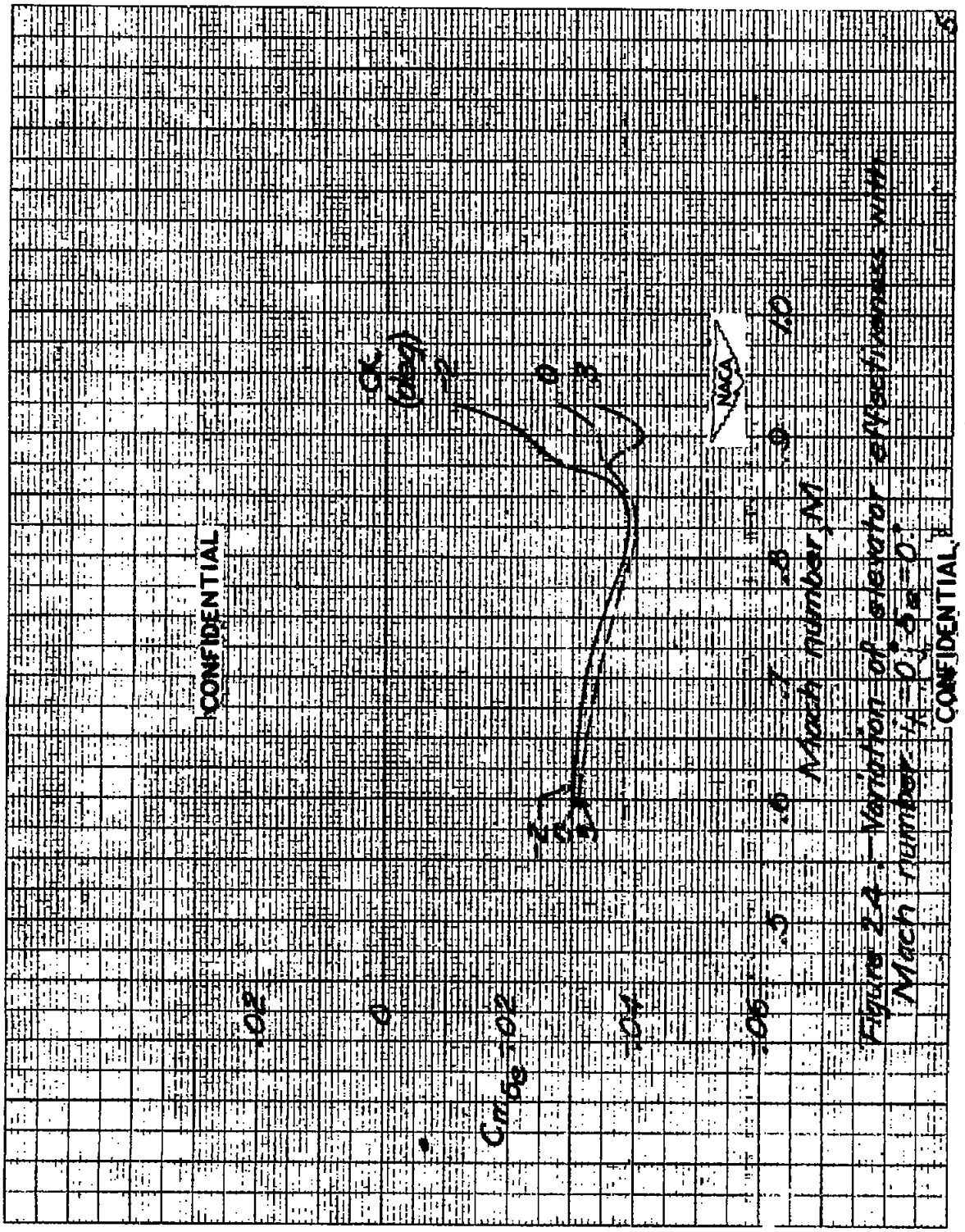

Figure 24.- Variation of elevator effectiveness with Mach number at $\alpha_t = 0.1°$, $\delta_e = 0°$.

Figure 25.- Variation of rate of change of pitching-moment coefficient with change in stabilizer setting with Mach number. $\alpha_c = 0°$; $\delta_e = 0°$.